Bull Volcanol (2012) 74:163–186
DOI 10.1007/s00445-011-0506-8

RESEARCH ARTICLE

Origins and energetics of maar volcanoes: examples from the ultrapotassic Sabatini Volcanic District (Roman Province, Central Italy)

Gianluca Sottili · Danilo M. Palladino · Mario Gaeta · Matteo Masotta

Received: 15 January 2011 / Accepted: 26 May 2011 / Published online: 23 June 2011

Abstract Maar volcanoes represent a common volcano type which is produced by the explosive interaction of magma with external water. Here, we provide information on a number of maars in the ultrapotassic Sabatini Volcanic District (SVD, Roman Province) as young as ~90 ka. The SVD maars are characterised in terms of crater and ejecta ring morphologies, eruptive successions and magma compositions, in light of the local substrate settings, with the aim of assessing magma–water interaction conditions, eruption energetics and genetic mechanisms. Feeder magmas spanned the whole SVD differentiation trend from trachybasalts–shoshonites to phonolites. From the ejected lithic fragments from aquifer rocks, the range of depth of magma–water explosive interaction is estimated to have been mostly at ~400–600 m below ground level, with a single occurrence of surficial interaction in palustrine–lacustrine environment. In particular, the interaction with external water may have triggered the explosive behaviour of poorly differentiated magmas, whereas it may have acted only as a late controlling factor of the degree of fragmentation and eruption style for the most differentiated magma batches during low-flux ascent in an incipiently fragmented state. Crater sizes, ejecta volumes and ballistic data allow a reconstruction of the energy budget of SVD maar-forming eruptions. Erupted tephra volumes from either monogenetic or polygenetic maars ranged 0.004–0.07 km^3 during individual maar-forming eruptions, with corresponding total magma thermal energies of 8×10^{15}–4×10^{17} J. Based on energy partitioning and volume balance of erupted magmas and lithic fractions vs. crater holes, we consider the different contributions of explosive excavation of the substrate vs. subsidence in forming the SVD maar craters. Following available models based on crater sizes, highly variable fractions (5–50%) of the magma thermal energies would have been required for crater excavation. It appears that subsidence may have played a major role in some SVD maars characterised by low lithic contents, whilst substrate excavation became increasingly significant with increasing degrees of aquifer fragmentation.

Keywords Maar · Eruption energy · Crater excavation · Crater subsidence · Hydromagmatism · Potassic volcanism

Editorial responsibility: M. Manga

G. Sottili · D. M. Palladino (✉) · M. Gaeta · M. Masotta
Dipartimento di Scienze della Terra, Sapienza-Università di Roma,
P.le Aldo Moro 5,
00185 Rome, Italy
e-mail: danilo.palladino@uniroma1.it

G. Sottili
Istituto di Geologia Ambientale e Geoingegneria-CNR,
Rome, Italy

Introduction

Maar volcanoes, among the most common volcanic landforms on Earth, result from hydromagmatic eruptions which are driven by the explosive interaction of magma with external water (i.e. groundwater and/or shallow bodies of sea or lake water), understood as a variety of molten fuel–coolant interaction (Wohletz and Sheridan 1983; Wohletz 1986). Maar volcanoes can derive from either single (monogenetic maars) or multiple (polygenetic maars) eruptive events separated by significant intervals of inactivity (e.g. Ollier 1967; Lorenz 1973; Németh 2010; White and Ross, 2011). Hydromagmatic activity is generally characterised by high degrees of magma fragmentation, although different interaction sites and changes in the

relative masses of water and magma interacting explosively may result in a spectrum of eruption efficiency, eruptive styles and emplacement mechanisms, including phreatic, phreatomagmatic (i.e. interaction occurs with aquifers) and Surtseyan (i.e. interaction occurs in submarine or sublacustrine environments) activities (e.g. Walker and Croasdale 1972; Wohletz 1986; Houghton et al. 1996, 2000; White and Houghton 2000; Büttner et al. 2002; Carrasco-Núñez et al. 2007), often associated with magmatic activities unmodified by water (usually effusive, Hawaiian and Strombolian; the terms Vulcanian and Phreatoplinian are also used in some cases, ambiguously, to refer to hydromagmatic eruption styles). Even during individual eruptive events, varying mechanical efficiencies of magma–water explosive interactions (Wohletz 1986), and/or shifts between hydromagmatic and magmatic phases, may result into a variety of transitions from wet surge (i.e. containing saturated steam), to dry surge (i.e. with superheated vapour), to scoria fallout activity where magma fragmentation is dominantly driven by the exsolution of magmatic gases. In addition, different substrate and aquifer properties (e.g. soft vs. hard lithologies, fracture vs. pore permeability) can control the activity style and the overall shape of a maar–diatreme volcano, including its deposit architecture and root zone system (e.g. Lorenz 2003; Auer et al. 2007; Ross et al. 2008, 2011; Németh et al. 2010).

Maar-forming eruptions are quite common in a variety of geo-volcanological settings and are fed by a wide range of magmas, with mafic (most commonly) to silicic, either subalkaline or highly alkaline, compositions (e.g. Lorenz 2007; Austin-Erickson et al. 2008; Sottili et al. 2009). Generally, the compositional and physical characteristics of magma, such as viscosity and volatile content, are considered to play a primary role in controlling the efficiency of hydromagmatic interaction (e.g. Houghton et al. 2000). Alternative views (e.g. Lorenz 2007) propose that the heat of magma, rather than other chemical–physical properties, is the main factor controlling the characteristic explosive behaviour of maar volcanoes. Recently, evidence from experiments on rhyolitic melts (Austin-Erickson et al. 2008) suggests different behaviour of high-silica, viscous melts with respect to mafic, low-viscosity melts during explosive interaction with external water and the resulting magma fragmentation. In particular, stress-induced fracturing of highly viscous shearing magmas may lead to a critical magma–water interface growth, thus promoting molten fuel–coolant interaction even for viscous silicic magmas. Experimental evidence for interactions involving high-silica compositions is in good accord with field evidence from pyroclastic successions of rhyolitic tuff rings (Austin-Erickson et al. 2008; Zimmer et al. 2010).

Hydromagmatic activity has been common during Quaternary potassic volcanism of the Roman and Campanian Provinces (Central Italy). It has involved a wide compositional spectrum of potassic magmas (from 42 to >60 wt.% SiO_2) and ranged in scale from maar-forming events to large-scale pyroclastic flow eruptions (Mastrolorenzo et al. 2001; Palladino et al. 2001; Giaccio et al. 2007; Sottili et al. 2009; Taddeucci et al. 2010). Here, we report on maar volcanoes in the Sabatini Volcanic District (SVD; Fig. 1) which illustrate the relationships among relevant maar characteristics (i.e. crater size, ejecta volume, explosion depth) and energetics (modes of eruption energy release, changes of eruptive styles) with respect to the different magma compositions and the local geological–structural and hydrogeological settings. In this regard, maar activity is also compared with that of coexisting small-scale Strombolian/effusive centres to assess the possible factors controlling the dominant eruption character.

The only previously available study on specific SVD hydromagmatic centres (de Rita and Zanetti 1986) focused on the degree of magma–water explosive interaction as related to the local substrate characteristics, whilst Sottili et al. (2010a) provided a general stratigraphic and $^{40}Ar/^{39}Ar$ geochronologic setting for most of the SVD maars. New field and laboratory data on the eruption successions show that SVD hydromagmatic centres encompass a wide variety of crater sizes and morphologies, deposit architectures and subsurface rock types, suggesting in turn different depths and modes of magma–water explosive interaction. In a few cases, the occurrence of intervening paleosols indicates a polygenetic origin of some maars. Also, changing textural and compositional features of juvenile eruption products, which range from tephritic leucitite to phonolite rock types (~47–59 wt.% SiO_2 on a volatile-free basis), provide an interesting case study for evaluating the possible role of magma composition on the eruption characteristics. The aims of the present work were to provide insights into: (1) the different modes and efficiencies of hydromagmatic eruptions, which could be related to the different magma characteristics (e.g. chemistry and degree of porphyricity); (2) the depth of interaction of potassic magmas with aquifers and/or shallow waters through the evaluation of the depth and extent of entrainment of subsurface rock types (i.e. accessory vs. accidental lithic clasts); (3) the partition of the initial enthalpy of the feeder magmas into different forms of mechanical energies (e.g. associated with crater excavation and ballistic ejection); and (4) the mechanisms for the origins of maars (i.e. explosive excavation vs. subsidence) through the energy balance and the comparison of the ejecta volumes with the resulting crater sizes.

Geological setting

The SVD extends over an area of ~1,800 km^2, including part of the Rome metropolitan area, within the Quaternary Ultra-

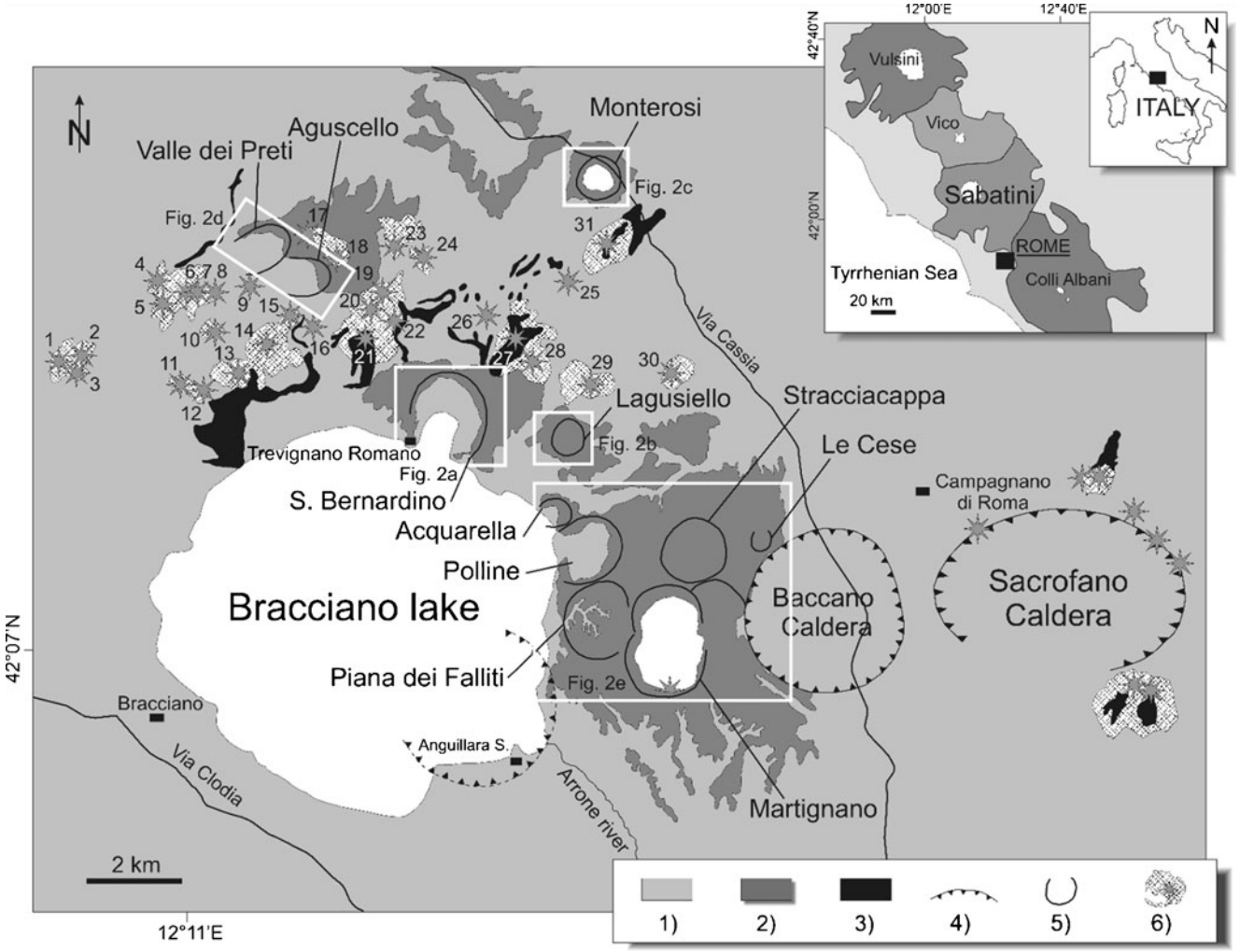

Fig. 1 Sketch map of the Sabatini Volcanic District showing the locations of monogenetic centres, including maars and scoria cones. *1* Pyroclastic products of the Sabatini Volcanic District; *2* Products of hydromagmatic activity; *3* Lava flows associated with scoria cones; *4* Caldera rim; *5* Maar crater rim; *6* Scoria cone (identification numbers refer to volume data reported in Table 2 and Fig. 9). Topographic features of hydromagmatic edifices are shown in Fig. 2. *Top right inset* Sabatini Volcanic District within the Quaternary Potassic Roman Province of central Italy

potassic Roman Province (Central Italy; Fig. 1). The SVD rock types represent a wide spectrum of ultrapotassic magma compositions extending from trachybasalts to trachytes/phonolites (e.g. Scherillo 1941; Cundari 1979; Campobasso et al. 1994; Conticelli et al. 1997; Sottili et al. 2004; Masotta et al. 2010). Available geo-volcanologic and geochronologic studies (e.g. Cioni et al. 1993; de Rita et al. 1993; Karner et al. 2001; Sottili et al. 2004, 2010a) show that the SVD volcanism encompassed a variety of eruption styles, intensities and magnitudes during three main periods of activity: (1) The oldest period (ca. 800–510 ka) took place from the Morlupo source area located in the eastern SVD sector and produced voluminous pyroclastic successions (including the major Tufo Giallo della Via Tiberina pyroclastic succession; Masotta et al. 2010); (2) during the intermediate SVD activity period, several Plinian fall deposits and the major Tufo Rosso a Scorie Nere were emplaced from the Southern Sabatini source area (ca. 510–420 ka); also, the Tufo di Bracciano (ca. 310 ka) and the Tufo Giallo di Sacrofano (285±1 ka) caldera-forming eruptions took place, respectively from the present-day Lake Bracciano and Sacrofano source areas; (3) the most recent activity (as young as ca. 90 ka) was sourced around the Bracciano and Sacrofano calderas, in the central–northern SVD area, and was characterised by dominant hydromagmatic and subordinate Strombolian/effusive eruptions from either scattered or clustered monogenetic centres. Strombolian and effusive centres were mostly aligned along the ring fault systems bordering the northern areas of the Bracciano and Sacrofano calderas. Hydromagmatic centres, the focus of this paper, mostly consist of tuff rings and subordinate tuff cones with maar-type craters, which formed within a NW/SE-trending, ~150-km^2-wide area in the central SVD, to the N

and E of present-day Lake Bracciano (Figs. 1, 2 and 3 and Table 1).

Several maars either still host small crater lakes (i.e. Martignano and Monterosi; Fig. 2) or were drained in historical times (Stracciacappa and Lagusiello) and represent the surface expression of a regional groundwater table in the volcanic terrains (Boni et al. 1986). Previous structural (de Rita and Sposato 1986) and gravimetric (Di Filippo and Toro 1993) studies, consistent with data from deep drilling for geothermal investigation (Funiciello et al. 1979) and lithic inclusions in the erupted products (de Rita and Zanetti 1986), suggest that maar-feeding magmas mostly interacted explosively with water reservoirs located in Meso-Cenozoic carbonate and siliciclastic horst areas, although in some cases the explosive interaction may have occurred with shallow surface waters.

Also, in light of new stratigraphic and geochronologic evidence (Sottili et al. 2010a), with implications for volcanic hazard in the Roman area, a detailed definition of the SVD maar products in terms of depositional features, eruption conditions and feeder magma systems is needed. Field and compositional aspects of the maar eruption products are described in "Results".

Methods

Laboratory analyses

Samples from juvenile clasts were investigated in order to characterise the geochemical features of the SVD maar feeder magmas. Microprobe analyses were performed on glasses and mineral phases at the CNR-Istituto di Geologia Ambientale e Geoingegneria (Rome, Italy) by a Cameca SX-50 EMP, equipped with five wavelength-dispersive spectrometers, using 15-kV accelerating voltage, 15-nA beam current, 10-μm beam diametre and 20-s counting time. The major elements of bulk samples were determined on glass beads at the XRF Laboratory of the Dipartimento di Scienze della Terra, Sapienza-Università di Roma. Matrix effects for major elements were corrected using the method of Franzini et al. (1972). Thin section backscattered (BSE) images of juvenile clasts were obtained by a Jeol FE-SEM 6500F, equipped with an energy-dispersive microanalysis system, at the Istituto Nazionale di Geofisica e Vulcanologia, Rome. SEM morphoscopy of juvenile lapilli and ash particles was determined by a FEI Quanta 400 SEM at the Dipartimento di Scienze della Terra, Sapienza-Università di Roma.

Reconstruction of maar eruption energetics

Field data, laboratory experiments and theoretical models have been used to assess energy partitioning during hydromagmatic eruptions (e.g. energy for magma and country rock fragmentation, crater excavation, pyroclast transport, seismicity, air waves, etc.; Shimozuru 1968; Wohletz and McQueen 1984; Wohletz 1986, 2002, 2003; Yokoyama et al. 1992; Sato and Taniguchi 1997; Taddeucci et al. 2010; Valentine et al. 2011). Here, we apply current models describing the relationships among crater size, range of ballistic ejecta and eruption energy (Sato and Taniguchi 1997; Goto et al. 2001; Yokoo et al. 2002; see Taddeucci et al. 2010 for a recent overview) in order to define quantitatively the energetic aspects of the SVD maar-forming events. In particular, we focus on a critical aspect highlighted by Taddeucci et al. (2010): the relationships of the energy budget vs. crater size, with general implications for the incremental growth vs. major explosion-dominated origin of maars.

Fig. 2 Present-day topographic features of the study maars (letters *a*–*e* refer to insets in Fig. 1) and locations of the cross-sections in Fig. 3. *1* Maar crater rim; *2* Sample locations for chemical analyses of juvenile clasts; *3* Sites of ballistic clast size measurements: To avoid ambiguity in cases of coalescing maars, *black arrows* point to the source of ballistic clasts as deduced from impact sags and other deposit features

Estimates of the eruption energy from maar crater size

According to available field explosion experiments (Goto et al. 2001), the final size of a maar crater reflects the mechanical energy released during the most intense explosion at an optimal depth, regardless of whether or not there are repeated explosive events (i.e. smaller energy explosions at the same location would not grow the existing crater, and cumulative energy would not affect the crater diametre). Following this approach, from maar crater size measurements, the "peak" energy associated with the climactic explosive phase of a maar-forming event could be derived (also cf. Taddeucci et al. 2010 for a recent application to the Colli Albani maars). Following Sato and Taniguchi (1997), Goto et al. (2001) also proposed an empirical relationship of crater-related energy, E_{cr}, vs. crater diametre, D:

$$E_{cr} = 10\mathrm{Exp}(\log D + 2.06)/0.32 \quad (1)$$

where E_{cr} is expressed in joules.

The average long and short axes of the SVD maar craters we studied (reported in Table 1) are approximated to the diametres of the circles that best fit the present-day crater areas, as measured by readings from 1:10,000 topographic maps (Fig. 2); these measurements are considered to have a ±10% error because of irregular shapes, crater erosion and filling.

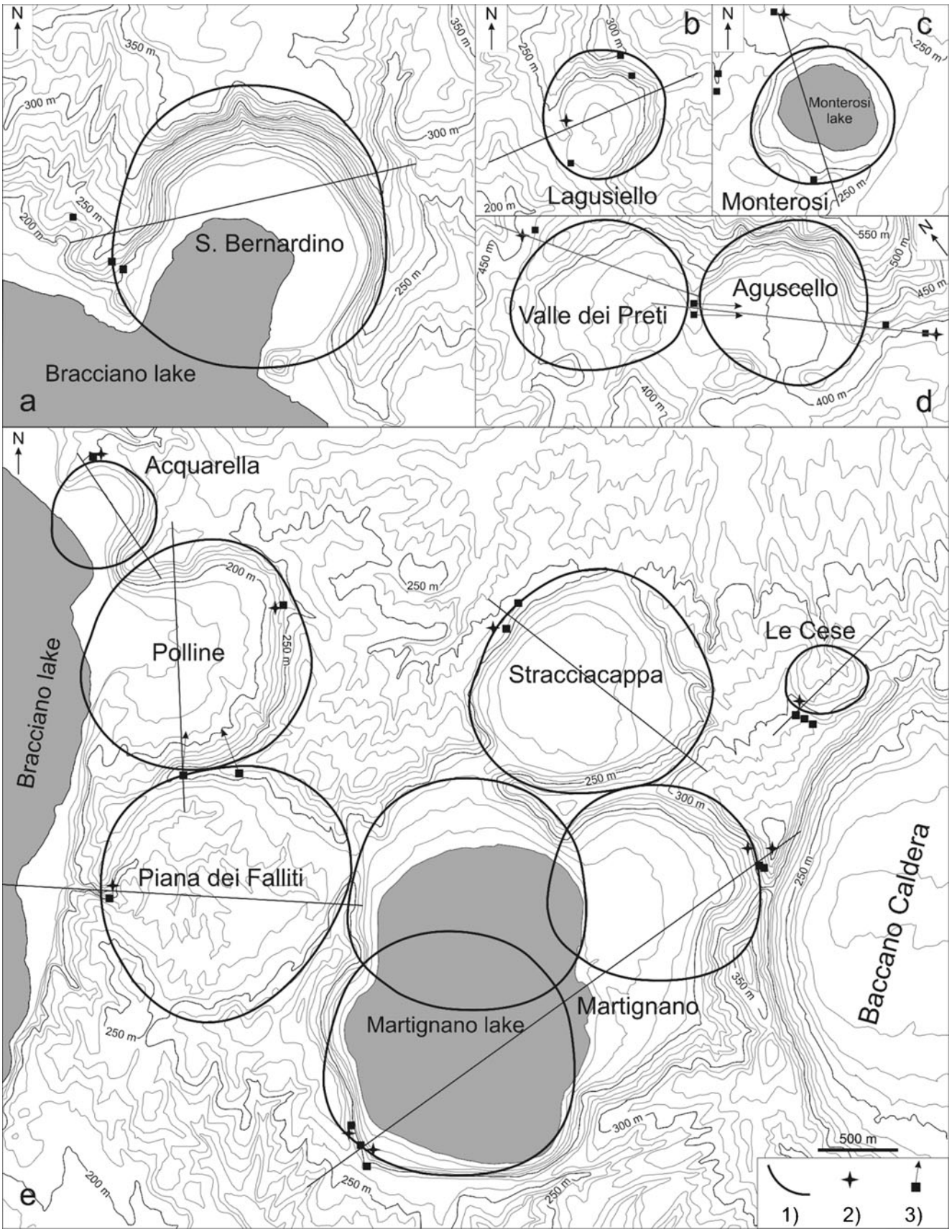
a
S. Bernardino
Bracciano lake
b
Lagusiello
c
Monterosi
Monterosi lake
d
Valle dei Preti
Aguscello
e
Acquarella
Polline
Piana dei Falliti
Stracciacappa
Le Cese
Martignano
Martignano lake
Bracciano lake
Baccano Caldera
500 m
1)
2)
3)

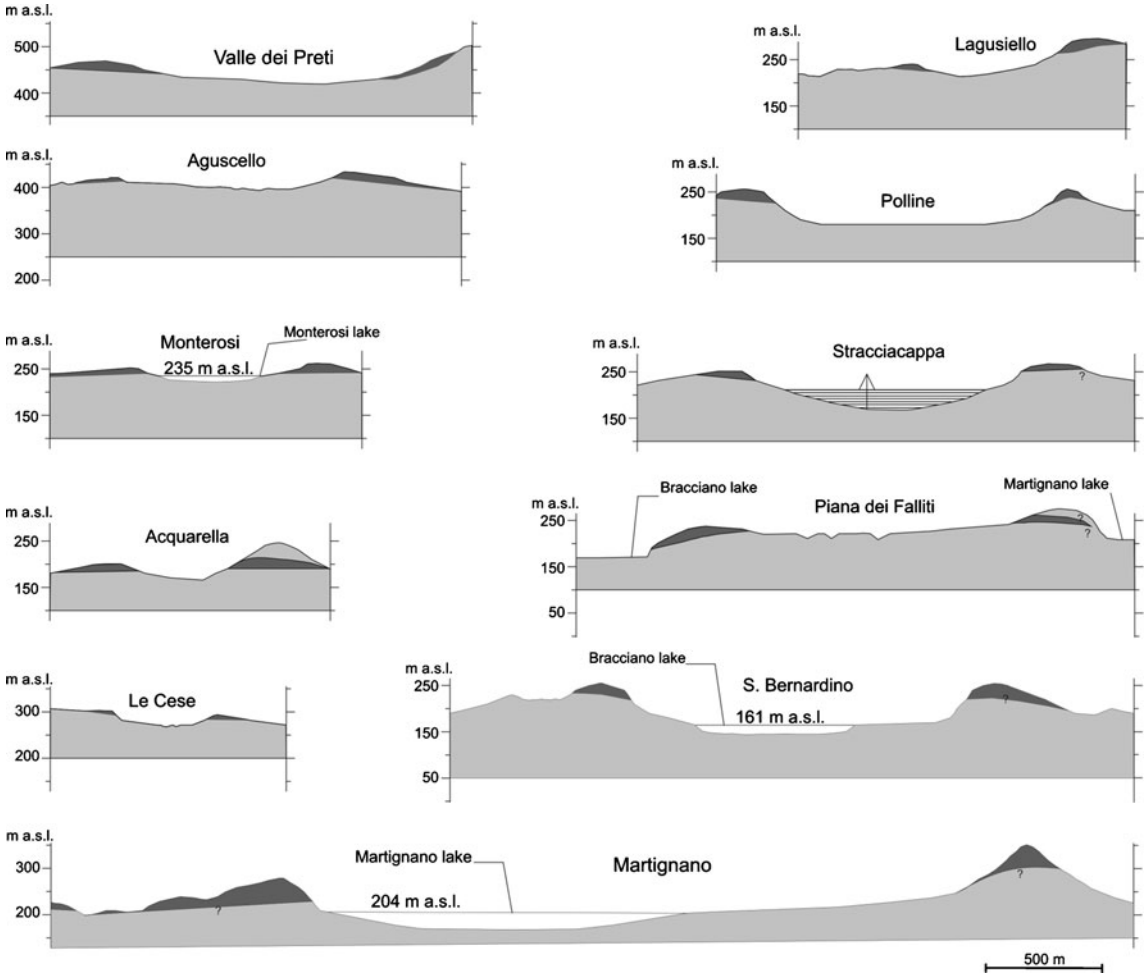

Fig. 3 Cross-sections of the study maars showing maar eruption products (*black filled*) and substrate rocks (*grey*; vertical exaggeration, ×2; see Fig. 2 for section locations). Thickness of lake sediments from drilling data (Giardini 2007) is also shown for the Stracciacappa maar. Pyroclastic deposits overlying the Acquarella and Piana dei Falliti maar eruption products are also shown (*grey*)

Estimates of the ejection velocity of ballistic clasts

The size and range of ballistically emplaced clasts in proximal pyroclastic deposits provide quantitative information on the ejection velocity at the source vent, as related to the energy of individual explosive pulses during transient explosive volcanic activity (e.g. Lorenz 1971; Fagents and Wilson 1993, 1996).

For each SVD maar, at representative outcrops, we measured the clast sizes of a set (usually some tens) of block- and boulder-sized ballistics, clearly associated with impact sags. For each clast, the average of the maximum and minimum axes was approximated to the radius, R. Following the approach of Fagents and Wilson (1993, 1996), we estimated the maximum gas expansion velocity at which ballistic clasts were ejected, u_0, from the maximum range of ballistic clasts of different sizes (assuming that they were vented from the crater's centre) by iterative calculation of their trajectories. First, we considered the drag force, F_d, affecting the block trajectories, as described by the relationship:

$$F_d = 0.5\rho_a\, C_d\, \pi R^2\, {u_0}^2 \quad (2)$$

where C_d is the drag coefficient and ρ_a is the air density. In the present analysis, we adopted C_d values from 0.5 to 1.3 by considering either spherical or cubic block shapes; ρ_a values were calculated at 20°C at the elevation above sea level of the take-off point. Then, we derived the gravitational force, F_g, acting on the blocks:

$$F_g = V\rho_b\, g \quad (3)$$

where V is the volume of a block assumed as a sphere with the diametre averaging the maximum and minimum block axes measured in the field, and ρ_b is the block density taken as 2,500 kg m^{-3}.

Finally, by considering that the maximum range of blocks of different sizes also depends on the launch angle

Table 1 Ages, morphological features and energy estimates for the SVD maars

Unit	Age (ka)	Sample label	Tephra ring volume (km^3, ±50%)	Magma thermal energy (J, ±50%)	Crater diameter (m, ±10%)	Crater excavation energy (J, ±10%)
Aguscello	296±3	AGU	0.011	4.1×10^{16}	1,070	8.0×10^{15}
Valle dei Preti	>296±3	VDP	0.024	9.2×10^{16}	1,010	6.7×10^{15}
S. Bernardino	≤172	SBD	0.035	1.3×10^{17}	1,720	3.5×10^{16}
Lagusiello	158±4	LAG	0.007	2.6×10^{16}	790	3.1×10^{15}
Monterosi	<150±4[a]; <134±33[b]	MTR	0.007	2.7×10^{16}	890	4.6×10^{15}
Acquarella		ACQ	0.009	3.5×10^{16}	650	1.7×10^{15}
Polline	<89±12	POL	0.016	6.2×10^{16}	1,470	2.2×10^{16}
Piana dei Falliti	89±12	PDF	0.015	5.7×10^{16}	1,620	2.9×10^{16}
Stracciacappa (upper)	97±4	USC	0.09	3.4×10^{17}	1,490	2.2×10^{16}
Stracciacappa (lower)		LSC			1,490(?)	2.2×10^{16}
Le Cese	95±5; 89±29	CES	0.002	7.9×10^{15}	560	1.1×10^{15}
Martignano (upper)	≤86	UMT	0.10	3.9×10^{17}	1,570	2.7×10^{16}
Martignano (middle)		MMT			1,490	2.2×10^{16}
Martignano (lower)		LMT			1,250	1.3×10^{16}

Volumes and magma thermal energies for the Stracciacappa and Martignano composite maars are calculated for the whole successions. Uncertainties with volume and related thermal energy calculations are at least a factor of 2. Input data for magma thermal energy calculations: magma temperature, 1,100°C; ambient temperature, 20°C; isobaric specific heat capacity of the magma, 1,450 J/kg K. Crater excavation energies are calculated from crater sizes through the empirical relationship by Goto et al. (2001). $^{40}Ar/^{39}Ar$ radiometric ages from Sottili et al. (2010a)

[a] $^{40}Ar/^{39}Ar$ radiometric ages from Laurenzi and Villa (1987)

[b] $^{40}Ar/^{39}Ar$ radiometric ages from Nappi and Mattioli (2003)

relative to horizontal, θ, we estimated ejection velocities, u_0, by varying θ from 30° to 60°.

Concerning the relationship of maximum ranges vs. block sizes, it is commonly accepted that ballistic blocks from maar eruptions show an overall decrease in diametre with distance from the vent. However, individual bursts may lead to the same initial ejection velocity of blocks irrespective of their size (Lorenz 1971), resulting in counterintuitive size–distance trends. For example, it was observed during the Ukinrek Êast Maar eruption, Alaska (Self et al. 1980), and the phreatic eruptions of the Inyo Craters, California (Mastin 1991), that the maximum ejection distance of small and large blocks was almost the same, with larger blocks occasionally ejected even to slightly larger distances than smaller ones. Assuming that ballistic blocks are ejected almost at the same initial velocity at the vent (and without considering possible vent migration within the footprint of the maar), this distribution can be explained because larger blocks can fly ballistically to slightly larger distances than smaller ones due to the lower effect of air drag (Lorenz 2007). As an example, the drag effect on block size was quantified here in the diametre vs. distance plot for ballistic blocks of spherical shape and density of 2,500 kg m^{-3}, at initial ejection velocities of 50, 100, 150 and 200 $m\,s^{-1}$ (see "Volume and energetics of maar eruptions"). Overall, this plot shows that small blocks need considerably higher u_0 than larger ones to be ejected to a given distance. In this study, the effect of the drag force on the range of ballistics of different sizes was thus considered for estimating u_0 from field measurements. For each maar case, we selected the three highest ejection velocities, as derived from the above theoretical modelling.

Volume of SVD monogenetic centres

The deposit volumes of tephra rings (reported in Table 1) were calculated based on the most complete exposures along the crater walls and scattered outcrops in relatively distal settings, assuming a thickness/distance decay of 1/10 broadly fitting the available radial cross-sections (Fig. 3). These values were then doubled to account for fine particle lost in distal areas, which are considered to amount to at least 50% of the total erupted products, considering the amount of ash loss during maar eruptions (e.g. Giaccio et al., 2007) and larger-scale hydromagmatic (e.g. Palladino et al., 2001) and magmatic (e.g. Sparks and Walker 1977; Ernst et al. 1996) eruptions. Maar crater volumes were obtained from readings from the 1:10,000 topographic maps by considering the present-day morphologies of the craters below the preexisting ground level. Due to the highly variable degree of compaction and abundance of country rock, even in the deposits of individual maars, a reliable conversion of the volumes of the erupted products

to magma volume (lithic-free dense rock equivalent, DRE) values was not obtained. However, based on crude estimations, in each case, we approximated the volume of erupted magma to that of the tephra ring (Table 1), considering that the uncertain evaluation of the distal ash loss is roughly counterbalanced by the density conversion factor and the lithic content required for DRE calculation.

For comparison, scoria cone volumes (Table 2) were calculated from topographic maps, relative to the preexisting surfaces, also taking into account possible co-eruptive lava effusions. In these cases, the volume of lavas erupted from central vents and/or fissures and breakouts (e.g. boccas located along cone slopes) was estimated from the areal extent and average thickness of the lava flow. For DRE conversion, we considered that the smaller fraction of ash loss relative to hydromagmatic centres was roughly balanced by the denser nature of proximal deposits.

Table 2 Volumes of SVD scoria cones in the study area, including associated lava flows (undetermined error related to irregular morphologies and limited ash loss)

Number	Scoria cone	Volume (km^3)
1	Monte Raschio	0.018
2	Lat. 42°10′37″, Long. 12°09′39″	0.005
3	Lat. 42°10′25″, Long. 12°09′36″	0.005
4	Monte Cavozza	0.003
5	Poggio Stracciacappello	0.010
6	Monte Termine	0.024
7	Lat. 42°11′05″, Long. 12°11′09″	0.010
8	Lat. 42°11′03″, Long. 12°11′32″	0.020
9	Monte Sassano	0.009
10	Monte Levo	0.004
11	Poggio dell'Oriolo	0.006
12	Poggio del Nespolo	0.021
13	Poggio le Vacche	0.039
14	Monte Capriglio	0.001
15	Lat. 42°10′57″, Long. 12°13′04″	0.001
16	Monte Riccio	0.008
17	Lat. 42°11′58″, Long. 12°13′27″	0.054
18	Monte Calvi	0.054
19	Monte Ferracatulo	0.008
20	Lat. 42°10′55″, Long. 12°14′17″	0.013
21	Monte Rocca Romana (315±14 ka[a])	0.120
22	Monte Rinaceto	0.024
23	Monte Guerrano	0.032
24	Poggio Tramontana	0.006
25	Monte del Nero	0.005
26	Monte Topino	0.001
27	Macchia di Monterosi	0.016
28	Monte Agliano	0.029
29	Monte dell'Olmo	0.013
30	Monte Pogliano	0.005
31	Monte Lucchetti	0.028

Numbers refer to the location map in Fig. 1

[a] $^{40}Ar/^{39}Ar$ radiometric age from Sottili et al. (2010a)

Componentry

Conventional grain size analyses by dry sieving techniques and determination of component abundances by weighting/counting (e.g. Cas and Wright 1987) were not applied to these pyroclastic successions, owing to the common, moderate to strong, lithification due to vapour phase zeolite crystallization. We developed an alternative approach (see Sottili et al. 2009 for details) to quantify the volume per cent of accidental and accessory lithic clasts from field-scale observation, by measuring the maximum axis lengths of all clasts coarser than 0.4 cm, exposed over a representative area of at least 8 m^2 for each eruption deposit. To obtain a homogeneous data set, clast size data were corrected by stereological conversion from 2D to 3D data by means of the "representative volume" stereological method (e.g. Sahagian and Proussevitch 1998).

Results

Field aspects and stratigraphy of the SVD maars

Here, we provide a description of the relevant field characteristics and new stratigraphic data of the SVD maars (see location in Fig. 1), along with interpretation of eruptive and emplacement modes, which where inferred from unambiguous textural features of deposits (e.g. sorting, grading pattern, clast shape, occurrence of tractional features such as planar- and cross-lamination, dune-bedding, imbrication of lithic clasts and traction carpets; e.g., Sohn and Cough 1989) and their relationships with paleotopography. From stratigraphic correlations, supported by componentry, minero-petrographic and chemical features (see below) and available $^{40}Ar/^{39}Ar$ radiometric data (Sottili et al. 2010a), it appears that the hydromagmatic activity at different source vents often overlapped, resulting in interfingering eruptive successions, clustered tuff ring morphologies and intersecting craters. Generally, lateral continuity of exposures is limited because of extensive erosion and vegetation, precluding a detailed reconstruction of lateral facies changes of deposits and paleotopography. Stratigraphic discontinuities among eruptive units from different source vents mostly occur as paleosols or, subordinately, as extensive erosional surfaces (e.g. see Palladino et al. 2010 for an application of integrated lithostratigraphic and unconformity-bounded stratigraphic approaches to Quaternary volcanic terrains). The polyge-

netic nature of specific maars was inferred from the occurrence of intervening stratigraphic discontinuities representative of significant temporal breaks (much greater than the duration of a maar-forming eruptive event) in the eruptive successions and/or coalescing crater morphologies.

Present-day crater morphologies and representative geological sections of the studied maars are reported in Figs. 2 and 3; crater sizes, tephra ring volumes and available geochronological data are summarized in Table 1.

Valle dei Preti maar

The Valle dei Preti and Aguscello (see below) craters are two coalescing maars developed a few kilometres north of present-day Lake Bracciano (Figs. 1 and 2). The proximal deposits of Valle dei Preti are partially preserved along the northern crater rim and mostly consist of massive, ash-supported, poorly sorted loose deposits containing decimetre-sized altered lava blocks. The most favourable outcrops (Fig. 4), located 200 m away from the northern crater rim, show a >4-m-thick complex eruption succession made up of massive to stratified clast-supported inferred fall deposits of dark grey scoria lapilli, enclosing ballistic lava blocks and boulders with impact sags, alternating in the lower–middle portions with greenish-light grey, planar to cross-laminated ash beds from pyroclastic surges, pinkish vesicular tuff layers, and centimetre- to decimetre-thick well sorted horizons of angular whitish pumice lapilli, interpreted as fall deposits bearing occasional accidental lithic clasts from the Meso-Cenozoic carbonate substrate.

Aguscello maar

A well-developed brown paleosol records a significant temporal break between the Aguscello and the underlying Valle dei Preti deposits. Locally, where the paleotopography dips >20° towards the Valle dei Preti crater, an up to 5-m-thick chaotic volcaniclastic deposit is also present below the paleosol. The Aguscello deposits (296±3 ka; Sottili et al. 2010a), a few hundred metres away from the present-day crater rim, show a stratified appearance due to alternating centimetre-to decimetre-thick planar- to cross-laminated ash layers and decimetre-thick massive, clast-supported scoria lapilli beds, rich in accessory lithic clasts with occasional

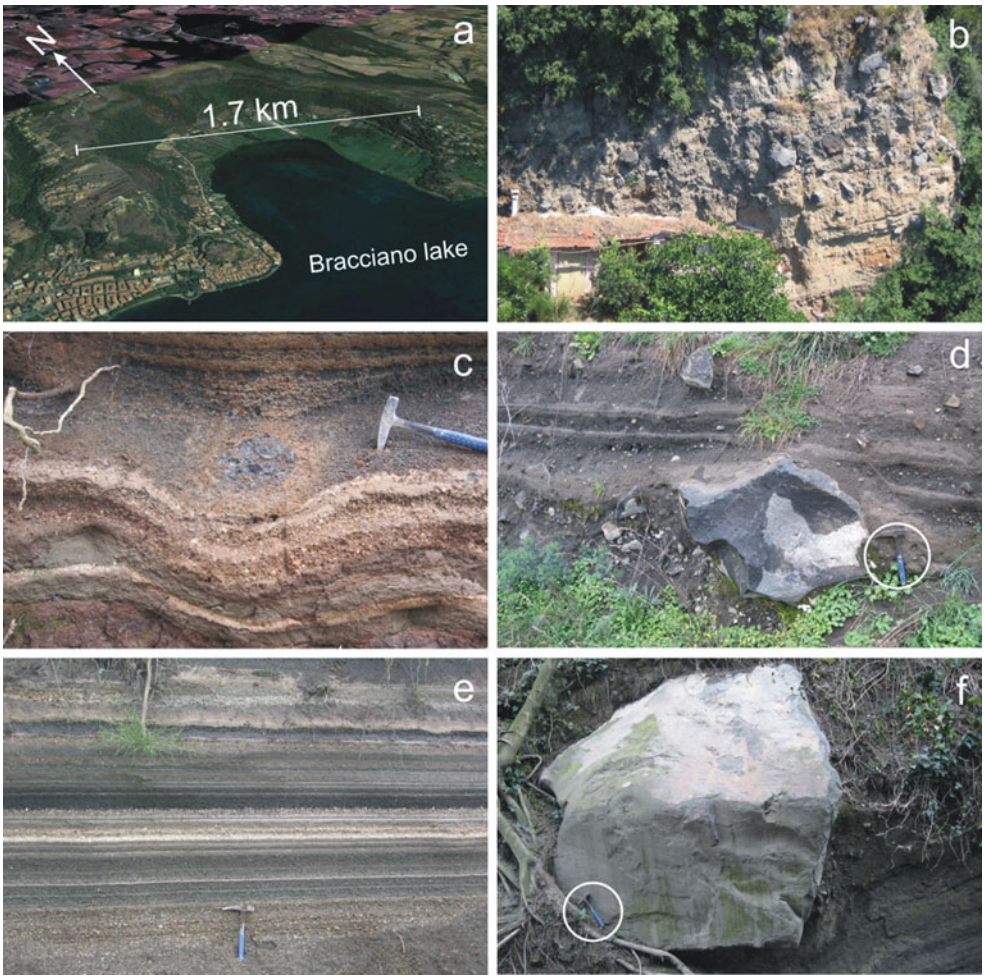

Fig. 4 Selected images from the SVD maars: **a** Aerial view of the S. Bernardino maar. **b** Lithic-rich proximal facies of the S. Bernardino maar eruption products exposed along the crater wall. **c** Ballistic lava block with impact sag in the Aguscello maar eruption products, approx. 400 m ESE from the present crater rim. **d** Near-vent Monterosi maar eruption products showing a ballistic lava boulder with impact sag, draped by ashy surge layers (*white circle* evidences hammer for scale). **e** Thinly stratified and laminated ash and lapilli succession from the Valle dei Preti maar. **f** Example of metre-sized ballistic lava boulder in the Stracciacappa maar eruption products, measured for ejection velocity estimates

impact sags (Fig. 4), thus indicating concomitant pyroclastic surge and fallout deposition. Juvenile clasts consist of dominant poorly vesicular, dark grey scoria in the middle and upper portions of the deposits, whilst moderately vesicular altered pumice clasts also occur in centimetre-thick layers interbedded with centimetre-thick ash layers towards the base of the succession. In proximal areas bordering the crater rim, a >10-m-thick massive ash matrix-supported, poorly sorted deposit from inferred pyroclastic current activity is present, also enclosing decimetre-sized ballistic lithic blocks. Locally, where the northward propagation of the pyroclastic current was limited by the presence of steep scoria cone flanks, the deposit is characterised by ash-poor lithic concentration zones showing clast imbrication.

S. Bernardino maar

The well-preserved S. Bernardino maar crater forms a bay (<15-m water depth) along the northern shore of the present Lake Bracciano (Fig. 4). Crater walls expose up to 20-m-thick proximal deposits, usually on top of a thick lava flow succession. Locally, a light brown thick paleosol marks the stratigraphic discontinuity between the S. Bernardino eruption products (≤172 ka; Sottili et al. 2010a) and the underlying Tufo di Bracciano main pyroclastic flow deposit (ca. 310 ka; Sottili et al. 2010a). The lack of evidence in the maar stratigraphy for significant hyatuses consistently indicates a monogenetic origin.

The S. Bernardino proximal deposits are massive and poorly sorted, and contain abundant, up to metre-sized, angular ballistic lava blocks in indurated ash matrix (Fig. 4). Scarce, poorly vesicular, dark grey juvenile clasts >1 cm in size contain abundant leucite phenocrysts. The 2-m-thick eruptive succession exposed 400–600 m away from the crater rim (near Monte Rocca Romana scoria cone) is characterised by 5- to 10-cm-thick beds of clast-supported, well sorted fall deposits containing angular dark grey scoria lapilli (up to 3 cm in size) and scarce lithic clasts (up to 2 cm) from the underlying lavas, alternating with 1- to 10-cm-thick fine- to coarse ash-grained surge beds, which commonly contain accretionary lapilli.

Lagusiello maar

The flat floor of the Lagusiello maar, located ~2 km NE of Lake Bracciano, once hosted a lake that was drained in historical time. Sottili et al. (2010a) report a radiometric age of 158±4 ka for the Lagusiello products cropping out around the horseshoe-shaped crater wall on top of a dark brown mature paleosol. In places, along the western crater wall, proximal deposits are as thick as 30 m: The 5-m-thick lower portion of the succession is well stratified due to alternating centimetre-thick clast-supported lithic-rich horizons, centimetre-thick well-sorted layers of leucite-bearing, poorly to moderately vesicular dark grey scoria lapilli, and millimetre- to centimetre-thick coarse ash layers with scoria lapilli swarms. Decimetre-sized angular ballistic lava blocks, with occasional impact sags, are also present. The upper portion of the succession is poorly exposed along the northern and eastern crater rims and is represented by massive and poorly sorted deposits containing decimetre- to metre-sized angular lava ballistics and scarce juvenile dark scoria lapilli in indurated ash matrix.

Monterosi maar

This well-preserved maar is located at the northern end of the SVD and hosts a small lake. Although a reliable age is still lacking (Sottili et al. 2010a), the Monterosi maar-forming event followed both the Prato Fontana lava effusion (134±33 ka; Nappi and Mattioli 2003) and the Tufo Rosso a Scorie Nere Vicano major explosive eruption (150±4 ka; Laurenzi and Villa 1987) from the nearby Vico Volcanic District. The base of the Monterosi eruptive succession is exposed locally along the crater walls, approx. 3 m above the present-day lake surface. The most proximal facies consist of dominant massive, ash matrix-supported poorly sorted deposits bearing decimetre- to metre-sized angular lava blocks and boulders (Fig. 4), interbedded with decimetre-thick, massive, moderately sorted horizons rich in centimetre- to decimetre-sized angular blocks from the local Meso-Cenozoic flysch substrate, derived from pyroclastic current and fallout activities, respectively. Near-proximal exposures, i.e. within a few hundred metres from the crater rim, show a >4-m-thick succession of 0.1- to 0.5-m-thick clast-supported fall deposit horizons of dark grey scoria lapilli and bombs, also enclosing abundant angular decimetre-sized lava and centimetre-sized flysch ballistic clasts, alternating with ash–lapilli surge beds containing diffuse loose millimetre-sized clinopyroxene and leucite crystals.

Acquarella maar

The Acquarella maar developed along the eastern rim of the Bracciano depression. The present-day, partially preserved crater has a horseshoe shape, its western rim facing the lake being completely eroded. Relic morphologies suggest that it was originally a tuff cone edifice. The ~15-m-thick proximal pyroclastic succession overlies a mature, brown paleosol developed on the brecciated top of a lava flow and is characterised by massive to variably laminated ash deposits from pyroclastic surges, enclosing deeply altered juvenile scoria lapilli and ballistic lava blocks. In places, lenticular lithic-rich zones with imbricated lava clasts are

also observed. The upper portion of this succession is partially reworked. Field relationships along the southern crater rim indicate that the Acquarella activity predated that of the Polline eruptive centre (see below).

Polline maar

The Polline maar is also located along the present eastern shore of Lake Bracciano and partially intersects the Acquarella maar to the north. The horseshoe-shaped crater rim is eroded to the west, where the flat crater floor is partially occupied by the lake. An erosional contact with the underlying products from the Piana dei Falliti maar nearby (89±12 ka; Sottili et al. 2010a; see below), exposed along the southern crater wall, indicates that the Polline activity represents one of the most recent eruptive manifestations in the SVD. Along the northern and eastern crater wall exposures, the Polline eruption succession rests on top of a mature paleosol developed on older SVD volcanics, mostly lavas. The Polline proximal deposits show an overall thickness of ~10 m and a well-stratified appearance due to alternating centimetre- to decimetre-thick fine ash to coarse lapilli layers and coarser-grained beds rich in lithic blocks. Generally, ash layers are poorly consolidated and contain abundant loose leucite and clinopyroxene crystals. In places, tractional features, such as imbrication of coarse lapilli (accessory lithic and scarce juvenile scoria clasts) in fines-poor, lithic-rich subhorizontal lenses, indicate emplacement from pyroclastic currents, whereas impact sags associated with lava blocks and boulders provide evidence of concomitant ballistic fallout.

Piana dei Falliti maar

The Piana dei Falliti maar (89±12 ka; Sottili et al. 2010a) is located between the Bracciano and Martignano lakes. The crater fill is deeply dissected by a dendritic drainage network, as deep as 20 m, down to the local base level represented by the Bracciano lake surface. The Piana dei Falliti eruption products directly overlie a >3-m-thick light brown, clay-rich deposit of palustrine–lacustrine environment. The proximal eruptive succession is dominated by parallel- to cross-bedded ash–lapilli deposits containing abundant accretionary lapilli, emplaced by pyroclastic surges. Diffuse, up to metre-sized, ballistic lava boulders with impact sags are also present. A road cut along the western crater rim shows that, occasionally, ballistic blocks penetrated into the co-eruptive surge beds upon impact and sank into the underlying soft sediments. Associated whitish clay–silt deposits of lacustrine origin and poorly sorted chaotic volcaniclastic deposits (possibly from mass reworking of rim deposits into the crater) are locally observed upsection.

Stracciacappa maar

The Stracciacappa maar is located immediately to the north of the Martignano composite maar (see below). The well-preserved flat-floored crater hosted a lake until it was drained in AD 1834. Based on palynological studies, the oldest lacustrine sediments date back to ca. 60 ka (Giardini 2007), broadly consistent with the radiometric age of 97± 4 ka obtained by Sottili et al. (2010a) for the upper part of the maar eruption succession. The whole proximal succession, ~15-m-thick, is best exposed along a series of road cuts radial to the northern crater wall. An intervening immature paleosol at about 10 m from the base records a significant eruptive break and the polygenetic nature of the maar, although the craters cannot be distinguished from one another morphologically. The lower unit overlies a mature dark brown paleosol and dips 10–15° towards the crater centre, whilst the upper unit is either subhorizontal or dips more gently (~5°) towards the same direction. Both units are dominated by poorly sorted deposits with well-developed sandwave bedding and lenses of imbricated lava lapilli, providing evidence of emplacement from pyroclastic surges, associated with subordinate clast-supported and well-sorted horizons of dark grey angular scoria lapilli of fallout origin. Up to metre-sized ballistic lava boulders with impact sags are scattered throughout the deposits (Fig. 4). Previous studies, based on grain size and component data and SEM particle textures (de Rita and Zanetti 1986), recognized an overall transition from dry (tuff ring) to wet (tuff cone) phreatomagmatic activity during the evolution of the Stracciacappa centre.

Le Cese maar

This small horseshoe-shaped phreatomagmatic crater formed at 95±5 ka (Sottili et al. 2010a) immediately NW of the Baccano caldera. The proximal deposits of Le Cese crop out locally along the crater walls on top of an immature paleosol developed on the Baccano eruption products and are characterised by centimetre- to decimetre-thick fine to coarse ash-grained subhorizontal layers. The juvenile component is represented by poorly vesicular leucite+dark mica-bearing black scoria lapilli. Tractional features, such as cross-lamination and lenticular zones of imbricated lithic clasts, indicate emplacement by pyroclastic surges. The occurrence of isolated decimetre-sized lava blocks with impact sags indicate concomitant ballistic emplacement in this near-vent setting.

Martignano composite maar

The lake-hosting Martignano maar is located to the east of Lake Bracciano. Composite volcanic morphologies show at

least three coalescing craters, overall 2.5 km across. The occurrence of two immature paleosols and/or erosional unconformities in the proximal stratigraphic successions indicates a polygenetic evolution of the eruptive centre: In this work, we recognized at least three distinct eruptive units, informally referred to as lower, middle and upper Martignano, respectively. Overall, the Martignano eruption products crop out in an area of at least 16 km^2 around the present craters, as far as approx. 4 km away from crater rims.

Proximal deposits at least 30 m thick are exposed along the southern crater wall, on top of a dark brown paleosol developed on the products of a local scoria cone. Along the eastern crater wall, the lower unit rests unconformably on top of pyroclastic deposits from the nearby Baccano centre and is dominated by massive to variably laminated ash deposits from pyroclastic surges, enclosing decimetre-sized ballistic blocks from the carbonate substrate with impact sags. A few tens of metres away from crater rim, the lower unit is ~10 m thick and dips ~10–15° towards the Baccano caldera.

The middle Martignano unit is approx. 20 m thick in crater wall exposures, where it dips ~25–30° towards the crater centre. It is well stratified due to alternating centimetre- to decimetre-thick clast-supported lithic-rich horizons, well-sorted scoria lapilli fallout beds and coarse ash layers; decimetre-sized angular ballistic carbonate blocks are also present. A light brown immature paleosol marks the transition to the upper unit, dated at ≤86 ka (Sottili et al. 2010a). In proximal settings, the upper unit, at least 10 m thick, is made up of light grey ash deposits displaying a variety of bedforms, including sandwaves, typical of pyroclastic surge deposits. Accretionary lapilli are either dispersed in the ash matrix or concentrated in swarms. Scattered centimetre-sized volcanic and carbonate clasts coexist in the lower–middle portions of the unit. Lava inclusions increase in size and abundance towards the top of the succession, where scattered up to metre-sized ballistics with impact sags are present.

Juvenile clasts, usually not exceeding a few centimetres in size, change upsection from poorly vesicular dark grey to microvesicular and greenish-light grey. The phenocryst assemblages include variable proportions of leucite (often turned to analcime) and feldspars, and ubiquitous clinopyroxene and biotite.

Microtextural and compositional features of the juvenile eruption products

Petrography

The relevant petrographic features of the juvenile eruption products from the SVD maar deposits are reported in Table 3. On the grounds of microtextural features and mineral assemblages, four juvenile clast types can be recognized, as follows.

Clinopyroxenite This clast type only occurs in the upper Martignano unit and is characterised by relatively high porphyricity (porphyricity index, PI=20 vol.%) due to the occurrence of abundant millimetre-sized clinopyroxene, dark mica and olivine phenocrysts, associated with scarce spinel, in clinopyroxene-bearing nearly vitrophyric poorly vesicular groundmass (Fig. 5).

Leucite-tephrite This clast type, only found in the middle Martignano unit, displays low porphyricity (PI<10 vol.%) due to the occurrence of phenocrysts and glomerocrysts of millimetre-sized clinopyroxene, plagioclase and spinel. The poorly vesicular groundmass is made up of plagioclase, clinopyroxene and leucite, associated with scarce sanidine, spinel and glass (Fig. 5).

Tephritic leucitite This is the most common juvenile clast type in the SVD maar deposits and is characterised by prevailing leucite and clinopyroxene (Fig. 5), occurring

Table 3 Main petrographic features from thin section observations and chemical compositions of juvenile clasts in the SVD maar deposits (sample labels as in Table 1)

Juvenile rock type	Porphyritic index (vol.%)	Glass	Vesicles (vol.%)	Main phases	Other phases	Glass composition	Bulk composition	Sample label
Clinopyroxenite	~20	Abundant	5	Cpx	Ol, dark mica, Spl, glass	Bimodal: phonotephrite and phonolite	K-basalt	UMT1
Leucite-tephrite	~15	Scarce	5	Plg, Cpx, Lct	San, Amph, Spl, glass	Trachyte	Trachybasalt	MMT1
Tephritic leucitite	~7	Scarce	3–17	Lct, Cpx	Plg, San, Spl, glass	Bimodal: phonotephrite and phonolite	Phonotephrite to tephri-phonolite	LSC, MTR, AGU, POL, SBD, ACQ, USC, LAG, VDP2, CES
Phonolite	~10	Abundant to scarce	5–30	San, Lct	Cpx, Plg, dark mica, Spl, glass	Phonolite	Phonolite	LMT, MMT2, UMT2, UMT3, VDP1, PDF

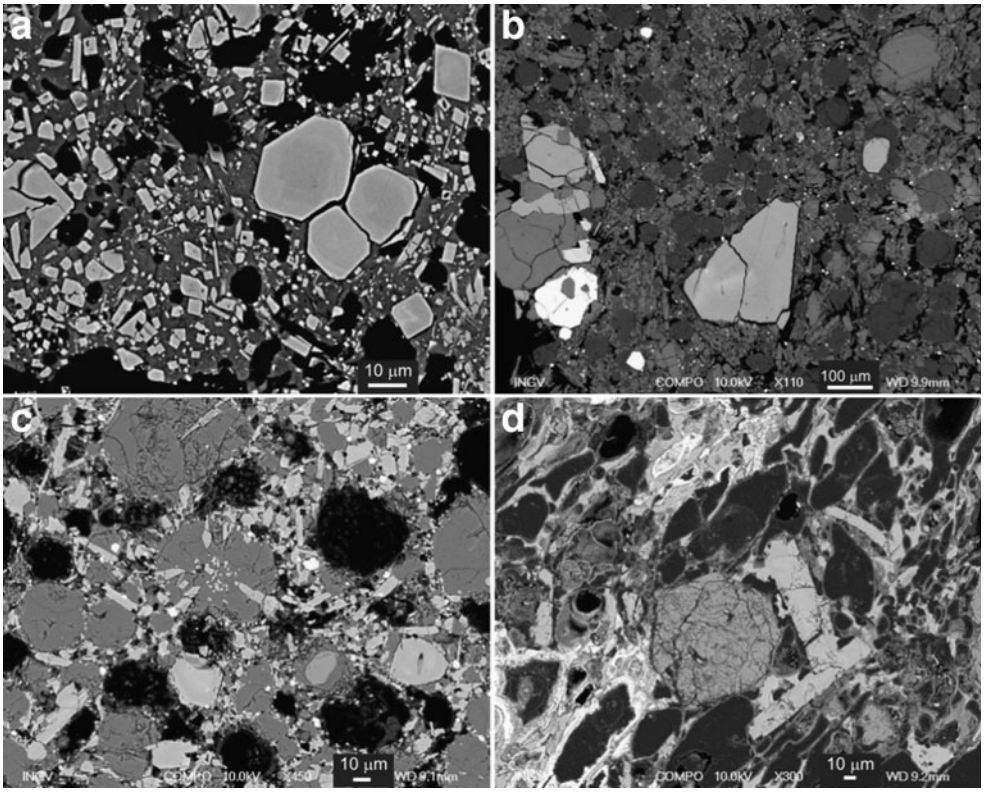

Fig. 5 Representative BSE-SEM microtextures of juvenile lapilli from selected hydromagmatic centres: **a** Clinopyroxenite rock type from the upper Martignano unit. **b** Leucite-tephrite from the middle Martignano unit. **c** Tephritic leucitite from Lagusiello. **d** Moderately vesicular phonolite from Valle dei Preti

both as sub-millimetre- to millimetre-sized phenocryst and groundmass phases. The degree of porphyricity is usually lower than 10–15 vol.%. The fine- to coarse-grained groundmass is scarcely vesicular and highly crystalline (leucite+clinopyroxene+plagioclase+spinel±sanidine) and contains scarce glass almost totally turned into zeolites.

Phonolite This juvenile clast type occurs in the Valle dei Preti, Piana dei Falliti and Martignano deposits. Compared with the above-reported rock types, it is characterised by higher vesicularity, a hypocrystalline (e.g. Piana dei Falliti) to glassy groundmass (e.g. Valle dei Preti, Fig. 5; VDP1 in Table 3) and by the occurrence of abundant sanidine phenocrysts, associated with leucite and scarce clinopyroxene, plagioclase, dark mica and spinel (PI ~ 10 vol.%).

Phase compositions

Glass The interstitial glass component in the juvenile clasts is commonly affected by post-depositional alteration into zeolites, with resulting Na–K substitution in the silicate network. For this reason, fresh glass compositions have been obtained in a few cases only (Table 4). Overall, glass compositions range from phonotephritic to phonolitic in the TAS diagram (Fig. 6). Parallel to the SVD liquid line of descent, as defined from bulk lava compositions (Conticelli et al. 1997), interstitial glasses in the studied eruption products are characterised by decreasing CaO contents with increasing SiO_2 (Fig. 6). In particular, the clinopyroxenite rock type contains two glass types: a scarce phonotephritic glass around olivine phenocrysts in the inner portion of the clasts and a more abundant phonolitic glass towards the clast rims. The interstitial glass in the leucite-tephrite rock type shows a peculiar trachytic composition outside the main compositional trend defined by the other maar glasses. We note, however, that the local occurrence of trachytic volcanics in the SVD has been previously reported (e.g. Morlupo Trachyte; Cioni et al. 1993). As it occurs in the clinopyroxenite, the tephritic leucitite products are characterised by a bimodal, either phonotephritic or phonolitic, glass composition. The latter glass composition also occurs in the phonolitic rock type. It is noteworthy that the volatile content in the interstitial glasses (Table 4), as deduced from the difference by 100% of the total of EMP analyses (Devine et al. 1995), is remarkably higher in the phonolite rock types than in tephritic leucitites, possibly indicating glass formation at different pressures.

Mineral phases Clinopyroxene is present in all the identified juvenile rock types, and its chemistry (Table 5) is a useful tool to discern chemical differences among the juvenile groups and to outline the evolution of maar-feeding magmas. Cr-bearing diopside in clinopyroxenite suggests that this clast type represents a rare snapshot of the most primitive magma involved in the SVD maar activity.

Table 4 Selected EMP analyses of interstitial glasses from maar juvenile eruption products (sample labels as in Table 1)

	Clinopyroxenite		Leucite-tephrite	Tephritic leucitite				Phonolite			
	UMT1	UMT1	MMT1	ACQ	LSC	USC	CES	UMT2	UMT3	LMT	VDP1
SiO_2	47.65	51.34	59.48	51.86	45.79	55.69	48.09	49.71	54.52	59.47	54.28
TiO_2	0.74	0.43	0.28	0.40	0.95	0.34	0.78	0.32	0.38	0.26	0.32
Al_2O_3	14.89	18.67	20.13	19.28	17.33	20.15	13.74	19.85	18.59	18.93	19.76
FeO_{tot}	6.45	3.91	1.41	3.43	8.94	3.64	6.59	2.36	2.85	1.24	2.78
MgO	3.76	0.77	0.24	1.81	1.99	0.32	5.97	0.12	0.37	0.09	0.25
MnO	0.17	0.13	0.08	0.05	0.28	0.22	0.17	0.09	0.08	0.04	0.15
CaO	12.38	5.09	4.36	5.81	10.27	4.37	13.76	7.04	3.60	2.45	3.05
Na_2O	2.21	3.40	5.23	1.33	4.23	6.22	3.42	2.63	3.29	2.14	6.41
K_2O	6.05	9.59	5.17	11.92	6.12	6.75	4.59	9.80	9.38	11.25	7.32
P_2O_5	0.29	0.10	0.44	0.24	0.53	0.46	0.39	0.09	0.03	0.05	0.01
F	0.30	0.48	0.15	0.04	0.61	0.62	0.26	0.49	0.29	0.02	0.03
Total	94.89	93.91	96.97	96.17	97.04	98.78	97.76	92.50	93.38	95.94	94.36

Clinopyroxenes in the leucite-tephrites and tephritic leucitites show a wide compositional range (Fig. 7) from diopside-rich compositions, similar to those occurring in the clinopyroxenite, to essenite–hedembergite–CaTschermak-rich compositions, like those occurring in the phonolites. Indeed, the diopside-poorest and essenite–hedembergite–CaTschermak-richest clinopyroxenes are found in the phonolites. Olivine is present in the clinopyroxenite only and shows a Fo_{86} composition. Leucite is characterised by a K/Na ratio from 15 to 23 and a FeO content ranging from 0.27 to 0.59 wt.%, although it is frequently turned to analcime. Plagioclase ranges from An_{90}-Ab_9-Or_1 in the leucite-tephrite and tephritic leucitites to An_{33}-Ab_{41}-Or_{26} in the phonolites. Sanidine ranges from Or_{69}-Ab_{20}-An_{11} to Or_{86}-Ab_{13}-An_1 in the leucite-tephrite and tephritic leucitites, whilst it shows an almost constant composition, $Or_{86\text{-}88}$-$Ab_{12\text{-}10}$-An_2, in the phonolites. Finally, dark mica is biotitic in composition and spinel is a Ti-bearing magnetite (TiO_2 ~ 6 wt.%).

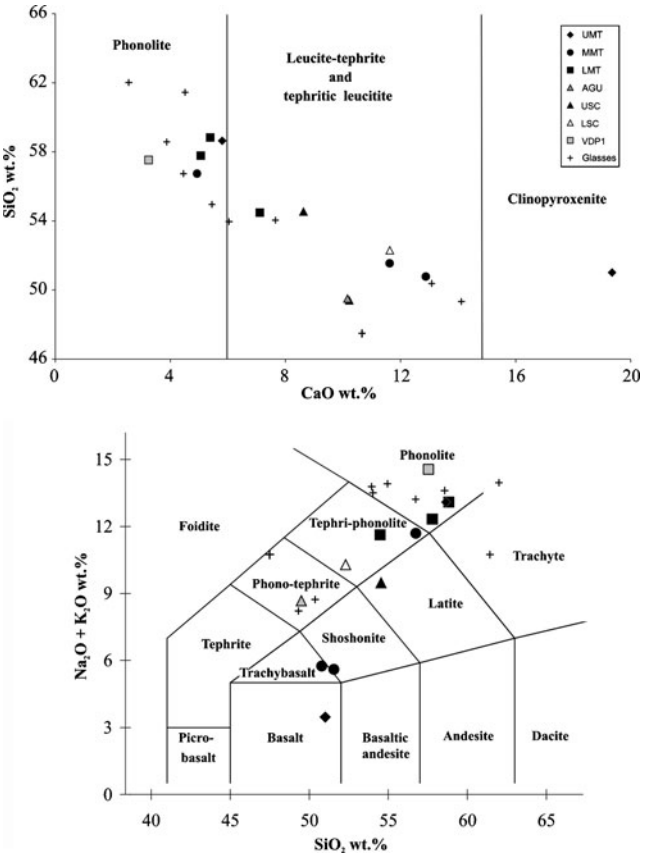

Fig. 6 *Top* CaO–SiO_2 plot of the study maar juvenile eruption products (see Table 1 for sample labels) defining the typical Roman Province magma differentiation trend towards phonolite rock types. *Bottom* TAS classification diagram of bulk compositions and interstitial glasses (symbols as in (**a**)) spanning a wide compositional range from basalts to phonolites

Bulk rock compositions

Based on bulk compositions (Table 6), the juvenile eruption products from SVD maars can be classified as ultrapotassic rock types (group III of Foley et al. 1987). In particular, clinopyroxenite, leucite-tephrite and tephritic leucitites represent primitive (MgO>3 wt.%) whilst phonolites represent differentiated (MgO<3 wt.%) ultrapotassic magmas. Overall, the available juvenile compositions define a negative correlation trend of SiO_2 vs. CaO contents (Fig. 6), indicating, consistent with the above petrographic features, that the clinopyroxenite and the phonolite are the most primitive and the most differentiated juvenile rock types, respectively. However, we must take into account that the clinopyroxenite, which plots in the basaltic TAS field (Fig. 6), partially reflects

Table 5 Selected EMP analyses of clinopyroxenes from maar juvenile eruption products (sample labels as in Table 1)

	Clinopyroxenite		Leucite-tephrite		Tephritic leucitite		Phonolite	
	UMT1		MMT1	MMT2	LSC		LMT	VDP1
SiO_2	52.23	53.88	43.04	45.11	52.46	42.92	47.69	40.54
TiO_2	0.32	0.30	2.05	1.59	0.39	1.76	0.83	1.88
Al_2O_3	1.97	1.80	8.50	6.42	2.47	10.21	5.65	9.16
FeO	3.44	3.40	11.86	11.78	3.74	11.90	9.01	17.54
MnO	0.01	0.11	0.27	0.47	0.09	0.24	0.22	1.04
MgO	16.68	17.40	9.98	9.38	16.37	9.27	11.71	4.96
CaO	23.75	23.53	23.14	23.61	24.84	23.49	23.69	22.82
Na_2O	0.18	0.18	0.45	0.56	0.14	0.43	0.25	0.69
K_2O	0.00	0.00	0.10	0.03	0.00	0.23	0.11	0.02
Cr_2O_3	0.86	0.36	0.02	0.00	0.28	0.00	0.00	0.00
Total	99.44	100.96	99.41	98.95	100.78	100.45	99.16	98.65
Formula on the basis of six oxygens								
Si	1.916	1.942	1.633	1.726	1.901	1.611	1.797	1.598
Ti	0.009	0.008	0.058	0.046	0.011	0.050	0.024	0.056
Al^{IV}	0.084	0.058	0.367	0.274	0.099	0.389	0.203	0.402
Al^{VI}	0.001	0.019	0.013	0.016	0.006	0.063	0.048	0.023
Fe^{3+}	0.053	0.025	0.274	0.210	0.074	0.268	0.132	0.322
Fe^{2+}	0.053	0.078	0.102	0.167	0.040	0.106	0.152	0.256
Mn	0.000	0.003	0.009	0.015	0.003	0.008	0.007	0.035
Mg	0.913	0.935	0.564	0.535	0.884	0.519	0.658	0.291
Ca	0.934	0.909	0.941	0.968	0.964	0.945	0.956	0.964
Na	0.013	0.013	0.033	0.042	0.010	0.031	0.018	0.053
K	0.000	0.000	0.005	0.002	0.000	0.011	0.005	0.001
Cr	0.025	0.010	0.001	0.000	0.008	0.000	0.000	0.000

the accumulation of clinopyroxene in a slightly more evolved magma, trachybasaltic or phonotephritic in composition. Juvenile bulk compositions, grouping the tephritic leucitite and phonolite rock types, define a main trend from the phonotephrite to the phonolite TAS field, paralleling the liquid line of descent of SVD magmas (Conticelli et al. 1997; Masotta et al. 2010). A subordinate vertical trend, from the basalt to the trachybasalt–shoshonite fields, is also detected within the most primitive compositions.

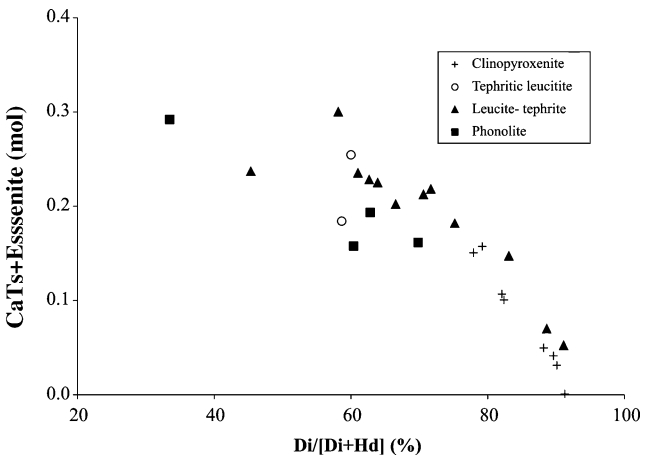

Fig. 7 Plot of clinopyroxene compositions (*Di* diopside, *Hd* hedembergite, *CaTs* CaTschermak) from juvenile scoria clasts paralleling the magma differentiation trend from clinopyroxenite to phonolite rock types

SEM microtextures

Microtextural features of the juvenile lapilli and ash fractions from SEM observations reveal two distinct groups of products. The first one (as best represented by the Monterosi eruption products) is characterised by poorly vesicular, blocky shaped, often deeply altered juvenile clasts with thick septa and occasional quench cracks. These features are typical for a dominantly hydromagmatic eruption style (e.g. Heiken and Wohletz 1985; Dellino and La Volpe 1996). In contrast, the juvenile fragments of the second group (as best represented by microvesicular greenish-light grey clasts in the Martignano deposits) show delicate contours, relatively high degrees of vesicularity, with high bubble density and complex bubble size

Table 6 Bulk compositions of maar juvenile eruption products obtained by XRF and EMP analyses (sample labels as in Table 1)

	Clinopyroxenite	Leucite-tephrite		Tephritic leucitite			Phonolite				
	UMT1[a]	MMT1[a]	MMT2[b]	LSC[a]	AGU[b]	USC[a]	LMTc[b]	LMT1[b]	LMT2[b]	MMT3[b]	UMT2[b]
SiO_2	50.66	50.83	49.84	52.29	48.76	54.34	56.49	56.11	53.32	55.43	55.17
TiO_2	0.65	0.90	0.75	0.93	0.87	0.63	0.32	0.46	0.55	0.57	0.31
Al_2O_3	18.16	19.30	17.34	18.67	15.97	19.69	18.47	18.73	18.76	19.26	18.10
Fe_2O_3	nd	nd	7.11	nd	6.69	nd	2.22	3.63	4.67	4.72	2.11
FeO	2.23	5.22	nd	2.15	2.13	4.48	nd	nd	nd	nd	nd
MgO	4.77	4.67	4.35	3.73	4.94	2.03	0.55	0.97	1.76	1.09	0.40
MnO	0.10	0.13	0.11	0.18	0.17	0.16	0.08	0.10	0.12	0.14	0.08
CaO	19.22	12.89	11.23	11.63	10.00	8.59	5.17	4.90	6.96	4.81	5.46
Na_2O	1.86	4.02	3.54	1.66	0.64	4.87	2.20	4.43	3.71	5.13	2.40
K_2O	1.59	1.74	1.88	8.63	7.91	4.57	10.37	7.54	7.67	6.30	9.92
P_2O_5	0.08	0.40	0.51	0.13	0.42	0.28	0.16	0.23	0.35	0.24	0.16
LOI	nd	nd	3.34	nd	1.50	nd	3.97	2.90	2.13	2.31	5.89
Total	99.32	100.10	100.00	100.00	100.00	99.64	100.00	100.00	100.00	100.00	100.00

[a] Bulk compositions of maar juvenile eruption products obtained by EMP analysis (total iron as FeO)

[b] Bulk compositions of maar juvenile eruption products obtained by XRF analysis (total iron as Fe_2O_3)

distribution even in the ash-sized particles. These features would be compatible with a shift towards a dominantly magmatic character (e.g. Houghton and Wilson 1989; Palladino and Taddeucci 1998), as inferred for the Baccano centre nearby (de Rita and Zanetti 1986). However, the superposition of a late hydromagmatic signature on a vesiculated and possibly incipiently fragmented magma is suggested by the occurrence of pervasive quench domains

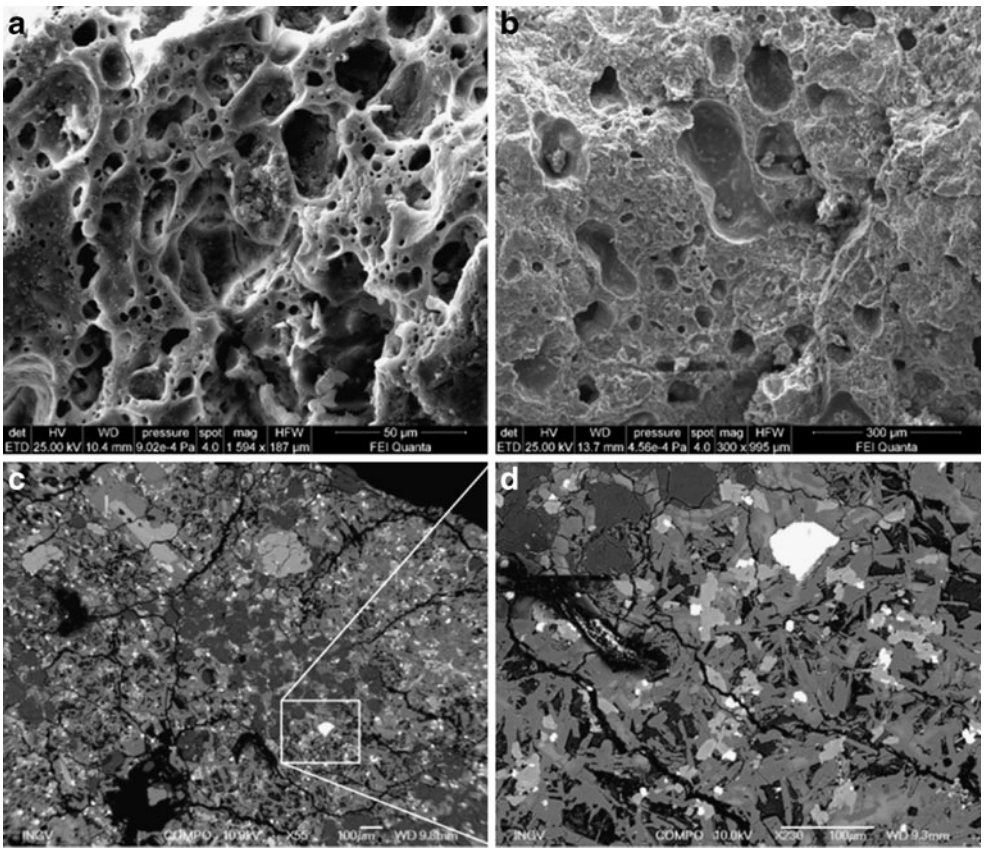

Fig. 8 SEM images of typical juvenile eruption products from the study SVD maars: **a** Moderately to highly vesicular lapilli from the upper Martignano unit showing complex vesiculation history with multiple nucleation events. **b** Poorly vesicular scoria clast with thick vesicle septa from Monterosi. **c** BSE image of a poorly vesicular, highly crystallized clast from Piana dei Falliti showing leucite-rich domains surrounded by sanidine-bearing domains with pervasive quench fractures, possibly recording an incipient fragmentation stage preceding the main fragmentation event during explosive magma–water interaction. **d** Detail of **c** showing domains of elongate sanidine microcrysts (*light grey*) and interstitial glass (*black*) cut by a pervasive fracture network

characterised by acicular sanidine microcrysts (e.g. Piana dei Falliti juvenile eruption products; Fig. 8).

Substrate clast types

The lithic clast content in phreatomagmatic deposits is considered to indicate the aquifer involved during explosive magma–water interaction and thus the depth of the interaction itself (Sheridan and Wohletz 1983; Barberi et al. 1988; White and Houghton 2000; Sottili et al. 2009). The investigated maar successions display rather monotonous lithic clast populations: Besides accessory lithic clasts, from dominant lava and subordinate pyroclastic units, which commonly occur in all cases, a significant proportion of accidental lithic clasts from the pre-volcanic Meso-Cenozoic sedimentary substrate is observed in a few cases only, i.e. ~10–65 vol.% in the Stracciacappa and Martignano maar deposits (Fig. 9). In the NW sector of the study area, below the Valle dei Preti, Aguscello, S. Bernardino, Lagusiello, Acquarella and Polline maars, volcanic aquifers (mainly consisting of fractured lavas and porous pyroclastic deposits) were mostly involved; occasionally, carbonate aquifers were also involved to a very limited extent (i.e. at Valle dei Preti). To the NE, below the isolated Monterosi maar, two aquifers interacted explosively with magma: a shallower one corresponding to the SVD volcanics and, possibly, a deeper one corresponding to the Meso-Cenozoic flysch rock types (Civitelli and Corda 1993). In fact, in the last case, the coarse size and angular shape of lithics, as well as the lack of evidence of thermal alteration, would suggest phreatomagmatic fragmentation of the aquifer rather than prolonged magma–wall rock heat exchange during entrainment in the ascending magma (cf. Sottili et al. 2010b). In the southeastern part, phreatomagmatic eruptions at Stracciacappa and, to a larger extent, at Martignano involved the Meso-Cenozoic carbonate aquifer in a horst structure (Mariotti 1993) during the early stages of the eruptions, followed by interactions at shallower depths with groundwater in the SVD volcanics. In one case, i.e. the Piana dei Falliti maar, besides the evidence of involvement of a shallow volcanic aquifer, the observed pre-eruptive stratigraphy also suggests the possible interaction of magma with surficial water in a palustrine–lacustrine environment.

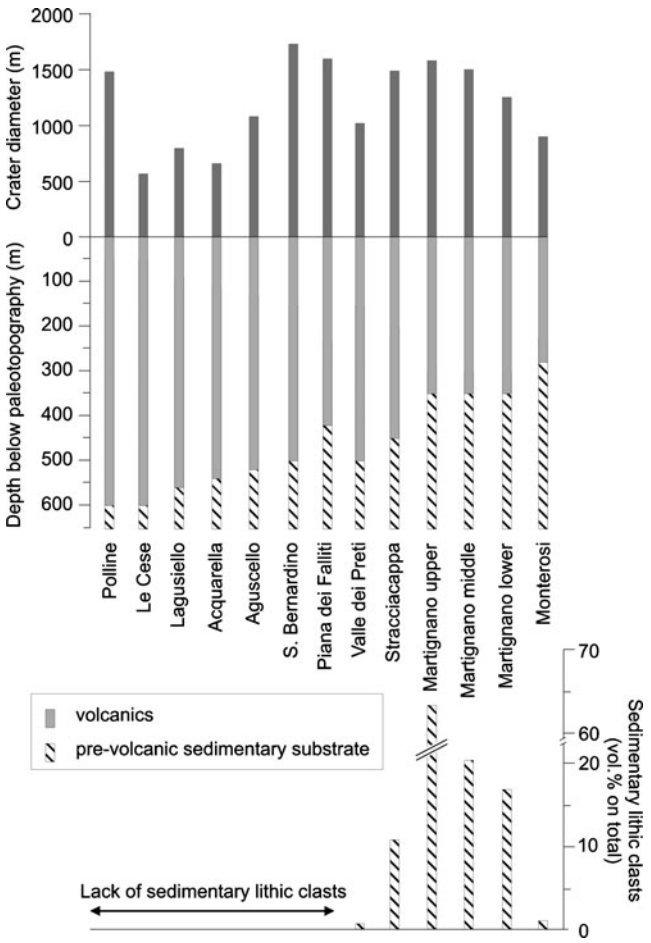

Fig. 9 Plots of crater diametres (±10%) and thickness of the volcanic pile (from available deep drilling and geophysical data, e.g. Funiciello et al. 1979; Di Filippo and Toro 1993) underlying the study SVD maars. The abundances of accidental lithic inclusions in the maar deposits are also reported (as volume per cent of the total lithic populations) in the lapilli and block fractions

Volume and energetics of SVD maar eruptions

Volume

The reconstruction of stratigraphy, lateral variations of deposit thickness and relict crater morphologies allow us to broadly estimate the volume of erupted products during individual SVD maar-forming events. The tephra volumes obtained for individual maar events (including the inferred distal ash loss; see "Methods" above) range from 0.004 km^3 (Le Cese) to 0.07 km^3 (S. Bernardino), with a cluster of values around 0.02–0.04 km^3 (Fig. 10). The largest edifice, the Martignano polygenetic maar, erupted a total volume of at least 0.2 km^3 of tephra during three main phases of activity. Calculations of related crater volumes, based on present topography (also taking into account the bathymetry of lake-hosting craters), yield a ratio of tephra volume vs. crater volume mostly between 0.5 and 1. The highly variable lithic proportions (up to a few tens of volume per cent) and densities of deposits (from loose to strongly consolidated) do not allow an accurate DRE conversion. However, as a rough estimate, the same ratio of 0.5–1 can be applied when referring to erupted magma vs. crater volumes.

For comparison, the volumes of SVD magmatic monogenetic centres (i.e. scoria cones and intervening co-eruptive lava flows) mostly range 0.005–0.06 km^3, with

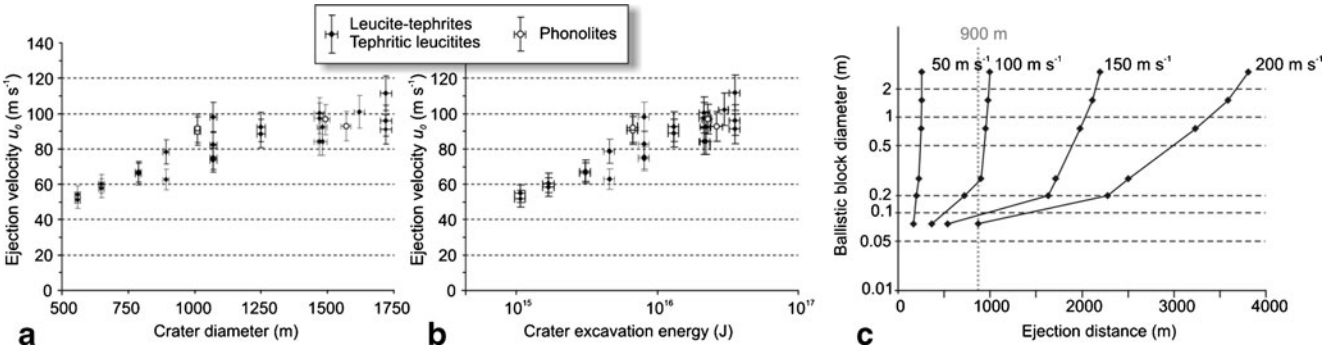

Fig. 10 Plots of the ejection velocity, u_0, of ballistic clasts vs. crater diametre (**a**) and energy required for crater excavation (**b**) for the SVD maars (error bars are also shown) following the model by Sato and Taniguchi (1997); see also Eq. 1 in the text. Plotted data are referred to the different rock types of the maar juvenile eruption products. **c** Theoretical plot of clast diametre vs. ejection distance for spherical ballistic clasts with density of 2,500 kg m^{-3} for different initial ejection velocities (50–200 ms^{-1}). For example, to reach a distance of 900 m from the vent, the ejection velocities required for a 10- and a 30-cm-sized ballistic clast are 150 and 100 ms^{-1}, respectively, due to drag effect (see "Methods")

the noticeable exception of Monte Rocca Romana (315± 14 ka, Sottili et al. 2010a; 609 m a.s.l., the highest elevation in the SVD), which attains 0.12 km^3 in volume (Fig. 11, Table 1).

Ejection velocity of ballistic clasts

Commonly, during SVD maar-forming events, ballistic blocks and boulders were ejected from the eruption vents and impacted on the growing tephra rings within several hundred metres from crater centre (Fig. 2). They mostly consist of angular or blocky shaped lava and subordinate sedimentary rocks from the pre-volcanic substrate, with those measured ranging from 10 cm to 2 m in size.

The three highest maximum ejection velocities (u_0) obtained for each maar crater yield values ranging from 50 to 110 m/s. The error associated with u_0 values is ±7–8%, as related to the range of input parameters adopted for calculations (i.e. launch angle θ ranging 30–60°, drag coefficient, C_d, ranging 0.5–1.3 for spherical or cubic block shapes; see "Methods"). Besides the uncertainty in the ballistic sources (here assumed as the maar crater centres), overall, the diametre vs. distance plot (Fig. 10) shows that small blocks need considerably higher ejection velocities than larger ones to reach a given ejection distance due to the effect of the drag force. Figure 10 also illustrates a broad positive correlation of the maximum ejection velocity of ballistics, u_0, with maar crater size.

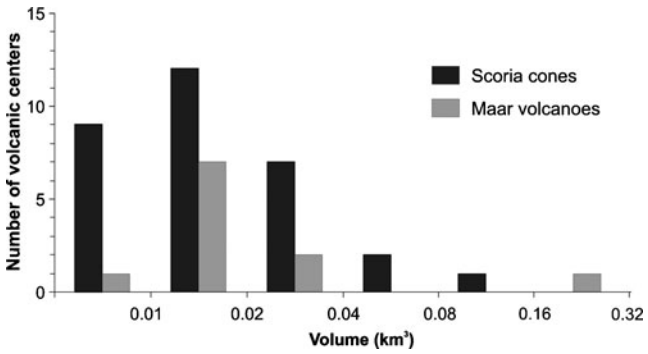

Fig. 11 Plot of volume distribution of juvenile eruption products (DRE) of individual maar volcanoes (based on present-day tephra ring, including inferred distal ash loss) and other monogenetic centres (i.e. scoria cones) vs. number of centres in the SVD. Although prevailing in number, scoria cones (including associated lava flows) show a volume distribution similar to that of maars

Crater excavation energy

Following the above-reported models that assume that maar craters are essentially explosively produced (i.e. without considering a significant component of subsidence), the energies associated with crater excavation, E_{cr}, estimated from Eq. 1, range from 1.1×10^{15} to 3.5×10^{16} J for the SVD case studies (Table 1). In comparison, the estimated mechanical energies required for crater excavation averaged 10^{12} J during the Usu 2000 phreatic explosions, Japan (Yokoo et al. 2002), whilst about 10^{13} J were released during individual phreatomagmatic eruptions at La Fossa di Vulcano, Italy (Büttner et al. 2002). Peak energies associated with crater excavation in the order of 10^{15}–10^{17} J are reported for the ultrapotassic maars in the Colli Albani Volcanic District, Roman Province (Taddeucci et al. 2010). For the SVD maars, E_{cr} also shows a broad positive correlation with the ejection velocity of ballistics (Fig. 10).

Discussion: conditions of magma–water explosive interaction

Hydromagmatic activity represents an important aspect in the SVD history and, particularly, during the most recent eruptive period until at least 90 ka. In this work, we have

characterised a representative set of SVD maars in terms of crater morphologies, deposit features and magma compositions with the aim of assessing magma–water explosive interaction conditions, eruption energetics and maar origins. Here, we address the modes and efficiencies of hydromagmatic eruptions, as related to the different characteristics of the potassic magmas involved and the depth of explosive interaction of magmas with aquifers and/or shallow waters. In the concluding section, we infer the main processes that formed SVD maars in light of the energetics of maar-forming eruptions.

In terms of crater widths and volumes of erupted products (Table 1), the SVD maars plot within the size range typical of tuff ring edifices on Earth (crater diametres of 0.2–3 km, tephra volumes of 0.0001–1 km^3; Head et al. 1981; White and Ross 2011). The SVD maar eruption successions share the lithofacies association typical of maar volcanoes elsewhere, including loose to strongly lithified ash and lapilli deposits with a variety of bedforms (e.g. massive, planar- and low-angle cross-lamination, sand-waves), from repeated, either wet or dry surge episodes, and concomitant fallout phases. Generally, the craters are surrounded by gently outward-sloping tephra rings with relatively steep inward-dipping slopes (i.e. >30°). Undulating pre-eruptive topographies, characterised by negative and positive landforms of erosional and volcanic (i.e. scoria cones, calderas) origin, affected to variable extents the radial expansion of phreatomagmatic surges and, thus, the related deposit architectures.

Facies analyses of maar deposits and the almost ubiquitous presence of paleosols underneath suggest that SVD maars essentially formed in subaerial environments, with the possible exception of the Piana dei Falliti maar that developed in a palustrine–lacustrine environment.

The eruptive successions for nine eruptive centres do not provide evidence of intervening time breaks (e.g. paleosols or extensive erosional surfaces) within the deposits of individual maars, thus suggesting a monogenetic origin. On the other hand, the multi-phase evolution of the Martignano composite maar occurred through at least three eruptive cycles, with products of the most recent dated at ≤86 ka (Sottili et al. 2010a). The Stracciacappa maar represents another example of a polygenetic edifice developed during at least two eruptive cycles, the youngest one dated at 97± 4 ka (Sottili et al. 2010a). From a hazard perspective, although a clear temporal pattern of eruption sizes is not observed for the SVD maars (Table 1), we note that the Martignano and Stracciacappa polygenetic maars, which erupted ~60% of the total volume of magma emplaced during maar activity, are among the youngest volcanic centres in the SVD.

Two main deposit types can be recognized in the SVD maars, although with overlapping ranges of crater sizes and edifice morphologies. The first one (which occurs in the Aguscello, S. Bernardino, Lagusiello, Monterosi, Acquarella, Polline, Stracciacappa and Le Cese centres) is characterised by poorly vesicular dark grey–black scoria as the juvenile component, high lithic content (some tens of volume percent in proximal deposits) and well-developed bedforms; it originated from crystal-rich, relatively mafic magmas, dominated by leucite+clinopyroxene mineral assemblages. The second one (occurring at Valle dei Preti, Piana dei Falliti, and Martignano) typically has light-coloured microvesicular pumice as the juvenile component, relatively high ash content and low lithic clast abundance (a few units of volume per cent even in proximal exposures), and derived from slightly porphyritic, sanidine-bearing highly differentiated magmas, phonolitic in composition. In addition, SEM observations reveal typical hydromagmatic ash textures in the first group, as opposed to a prevailing magmatic signature in the second one (Fig. 8).

The above picture consistently indicates that the fragmentation of relatively mafic magmas, which more commonly produced small-scale scoria cones and lavas in the SVD (Conticelli et al. 1997), was essentially driven by the explosive interaction with groundwater during maar-forming events. On the other hand, SVD maar-forming events fed by highly differentiated phonolitic magmas were possibly driven by late-stage interaction of vesiculated (and partially fragmented?) SiO_2-rich magmas with groundwater and/or surface water, analogously to the trachytic–phonolitic hydromagmatism at Campi Flegrei (Mastrolorenzo et al. 2001). This inference is also in agreement with recent field and experimental evidence (Austin-Erickson et al. 2008) suggesting that high-SiO_2 highly viscous melts differ from low-SiO_2 low-viscosity melts in how they interact explosively with external water. It appears that stress-induced magma fracturing is a prerequisite that may lead to a critical magma–water interface growth, thus initiating phreatomagmatic explosions and enhancing brittle fragmentation of silicic magmas.

It thus appears that in the SVD maar events, for given orders of volumes involved (<0.1 km^3) and amounts of available magma heat energies, different magma characteristics (e.g. chemistry and degree of porphyricity and vesicularity) play a role in controlling the modes and efficiency of magma–water interaction (and thus the eruption style and resulting textures of eruption products), but have little effect on the mechanical energy release as deduced from maar crater size and ballistic ejection velocity.

In this regard, among the studied maars, the Valle dei Preti eruption products might best represent a trend towards dominantly magmatic activity related to the development of a small-scale caldera system, as also inferred for the Baccano centre nearby (de Rita and Zanetti 1986). We note

that trachytic–phonolitic magma batches one or two orders of magnitude larger in volume typically fed purely magmatic, sub-Plinian to Plinian and pyroclastic flow-forming events at SVD (Campobasso et al. 1994; Sottili et al. 2004; Masotta et al. 2010).

As a whole, the areal distribution of hydromagmatic vs. magmatic monogenetic centres in the SVD study area reflects how the local hydrogeological setting of the substrate controls any water interaction with the pre-eruptive magma feeder system (see also de Rita and Sposato 1986). Lithic clast data from hydromagmatic deposits, in light of available data on the thicknesses of subsurface lithologies (Fig. 9), allow a crude estimation that the likely depth of magma–water explosive interaction was on the order of a few hundred metres. In particular, the maar examples (seven cases) lacking lithic clasts from the sedimentary substrate indicate interaction depths <450–600 m below the paleotopography, whilst interaction occurred at >300–500 m depth for those examples containing pre-volcanic rocks (six cases), with the lower depth limit inferred to be controlled by the pressure boundary for the occurrence of molten fuel–coolant interaction (~10 MPa in subaqueous environments: Zimanowski and Büttner 2003; although this point is still theoretically and experimentally debated, e.g. Wohletz 2003). The main water reservoir located below the maar cluster area caused the tendency of small, SiO_2-poor magma batches to produce phreatomagmatic explosive eruptions. Concerning the SVD maars fed by differentiated SiO_2-rich magmas, the presence of external water may have acted as a late controlling factor of the degree of fragmentation and eruption style, provided that the ascending low-flux, small magma batches were in an appropriate intrinsic stage of incipient fragmentation and/or cracking that enhanced permeability and magma–water interaction interface (regarded as a major controlling factor of hydromagmatic explosivity; Trigila et al. 2007, Austin-Erickson et al. 2008). Even for vesicular magma, in this case, incipient fragmentation preceding water interaction is inferred because a small, continuous trachytic–phonolitic magma batch is more likely to cross an aquifer and/or shallow water without significant interaction and erupt effusively, as also testified by scattered occurrences of phonolitic lavas in the SVD (see chemical analyses in Conticelli et al. 1997).

We remark that the SVD differs from other ultrapotassic volcanic districts of the Roman Province where only SiO_2-poor magmas (i.e. ranging in composition from K basalts and trachybasalts in the Valle Latina to shoshonites–phonotephrites at Vulsini and K-foidites at Colli Albani; Dolfi et al. 2011; Palladino et al. 2010; Sottili et al. 2009) were involved in hydromagmatic activity. On the other hand, the SVD parallels the Campi Flegrei case, where both end members of the magma differentiation line (respectively SiO_2-poor trachybasalts–phonotephrites and SiO_2-rich trachytes-phonolites; Mastrolorenzo et al. 2001; De Astis et al. 2004) produced tuff cones and tuff rings typical of relatively small-scale hydromagmatic activity, although with inferred different modes and boundary conditions of magma–water interaction due to remarkably different rheological behaviours of interacting magmas. For example, a typical trachytic tuff ring in the Campi Flegrei, with 0.07 km^3 (DRE) of erupted products and peak mass discharge rate of 3.2×10^6 kg/s (Averno 2, Di Vito et al. 2010) is comparable in scale with the main SVD hydromagmatic centres.

The SVD maars thus provide an additional example of the occurrence of small-scale silicic hydromagmatic activity, which is increasingly supported by field and experimental evidence in the recent literature (e.g. Monte Pilato-Rocche Rosse, Lipari, Italy: Dellino and La Volpe 1995; Fyriplaka tuff ring, Milos, Greece: Campos Venuti and Rossi 1996; Toga tuff ring, Japan: Kano et al. 2002; Kano and Ohguchi 2009; Tepexitl tuff ring, Mexico: Austin-Erickson et al. 2008; Cerro Pinto tuff ring–dome complex, Mexico: Zimmer et al. 2010). On the other hand, we remark that trachytic–phonolithic explosive eruptions of much larger intensities and magnitudes at SVD and other volcanoes of the Roman Province lack evidence of a dominantly hydromagmatic style (e.g. Sottili et al. 2004, Masotta et al. 2010, Colucci et al. 2010, Palladino et al. 2010), thus suggesting that efficient water interaction for high-flux, highly viscous magmas is still not conclusively ascertained (also cf. Palladino et al. 2008 and reference therein) and requires further analytical, theoretical and experimental work.

Concluding remarks: eruption energetics and inferences on maar origin

A puzzling aspect concerns the estimate of the energy released during a maar-forming eruptive event, as related to the maar size. If the size of a maar crater is determined mainly by explosive ejection of material, and crater size increases with increasing explosive energy (as in Goto et al. 2001), then one might argue that the diametre of a maar records the most energetic explosive event during the eruptive lifetime. On these grounds, Taddeucci et al. (2010) found that the cumulative energy released during a maar-forming event, corresponding to the enthalpy associated with the total mass of erupted magma, and the "peak" energy release derived from maar crater size were of comparable orders of magnitude, as if the most (a few?) intense eruption phases with peak mass discharge rates released a dominant fraction of the cumulative energy and essentially controlled the crater size. This somehow ambiguous issue was attributed to a significant, or even dominant, magmatic component in the Colli Albani maar eruptions.

However, considering a prolonged magma discharge through the duration of typically hydromagmatic activity (usually days to weeks for observed events, e.g. Lorenz 2007; White and Ross 2011) during the whole period of maar eruptive activity, we note that it is unlikely that almost the total energy associated with a given mass of initial magma could be available during a single explosion responsible of a given crater size. Rather, the crater size must have a significant component that is not the result of excavation by a single explosion (see also Valentine et al. 2011).

The role of explosive excavation of the substrate (e.g. Goto et al. 2001) vs. incremental subsidence (e.g. Lorenz 1986) in determining maar crater evolution and size is still an open question, especially considering that exposed maar morphologies reflect to a very limited extent their complex subsurface structure and evolution (including the diatreme and root zone, e.g. Ross et al. 2008; White and Ross 2011). A key point lies in the comparison of the volume of the ejecta (i.e. magma+lithic fragments) and the volume of the crater that is cut into the pre-eruptive landscape. A crater volume that broadly matches the volume of lithic material incorporated in the erupted products might support an origin from explosive excavation (such as that which can occur in a phreatic event). Conversely, similar volumes of total erupted magma and crater would indicate a collapse origin (caldera-style) of the maar. In this case, the favourable geometry and shallow depth of the pre-eruptive magma storage system would allow a surface expression of similar volume to the evacuated magma due to roof collapse.

From a balance of the magma, lithic and crater volumes, we note that in some SVD maars that are characterised by low lithic contents relative to the crater size (e.g. Valle dei Preti, Piana dei Falliti, and Martignano), the role of subsidence appears more important than substrate excavation, also consistent with the significant magmatic signature of their juvenile eruption products. This, in turn, suggests shallow pre-eruptive magma reservoirs, consistent with the variable degrees of magma differentiation at SVD maars and previous inferences from data on the thermal interaction of maar feeder ultrapotassic magmas with carbonate and siliciclastic country rocks in the Roman Province (Gaeta et al. 2009; Peccerillo et al. 2010; Sottili et al. 2010b). It appears that crater excavation becomes more and more significant with increasing entrainment of lithic fragments from the aquifers (e.g. S. Bernardino, Monterosi, Stracciacappa maars).

In this regard, the energy associated with a specific maar crater size (if assuming that it essentially resulted from explosive excavation; Goto et al. 2001) is a highly variable fraction (approx. 5–50%; Table 1) of the enthalpy associated with the total magma (DRE) erupted. We note that high values of crater excavation energies vs. total magma thermal energies yield the above-noticed conflicting results on the energy partition during maar evolution, thus making unlikely that maars originate from a single or a few dominant explosive events. For example, the unlikely high fraction of energy required to produce the Piana dei Falliti maar crater (~50%), coupled with the low lithic content in the tuff rings deposits, supports a predominant subsidence component relative to the explosive excavation of the substrate. In contrast, relatively low fractions of energy, associated with high lithic contents (e.g. Monterosi), support the formation of a crater predominantly by explosive excavation during the most energetic hydromagmatic phases. On these grounds, most of the SVD case studies reveal that a variable combination of both excavation and subsidence is likely to have controlled the origins of the different maars.

Ballistic clast data provide further inferences on the energy released during discrete explosive pulses. In particular, the observed positive relationship of increasing ballistic ejection velocity with crater size and associated excavation energy (Fig. 10) indicate that, as expected, the highest ejection velocities are associated with the most intense explosive phases responsible for crater widening.

To better determine the mass/energy balance would require consideration of additional factors related to the space–time evolution of the root zone of a maar (i.e. development of the diatreme–debris system, migrating *foci* of discrete hydromagmatic explosions, substrate rock deformation, collapse of the tephra ring onto the crater floor, subsidence of the crater floor by compaction of the diatreme fill; cf. Lorenz 2007; Ross et al. 2008), which cannot be ascertained when dealing with young maar volcanoes.

Some quantitative insights into subsurface processes are provided by the volatile contents in the melts, as inferred from the interstitial glasses of common phonolitic composition found in the SVD maar juvenile eruption products with different bulk compositions (Table 4). In fact, phonolitic interstitial glasses in phonolite rock types show remarkably higher H_2O saturation pressures than in tephritic leucitites (i.e. 160–120 vs. 110–40 MPa, respectively, as calculated following Moore et al. 1998), thus indicating melt quenching at greater depth. These values constrain interpretations of the minimum quenching depth to approx. 6.5–1.5 km, which appears significantly greater than that inferred for explosive magma–aquifer interaction based on lithic inclusions in the SVD maar deposits and current views considering explosive magma–water interaction as a relatively shallow process. The obtained quench depth values may thus likely record early quenching of discrete magma domains undergoing stress-induced, non-explosive brecciation in the diatreme–debris system (Ross et al. 2008). Furthermore, we note that for each rock type, a

negative correlation exists for the depth of the melt/glass transition with the maar crater diametre (Table 1), thus possibly suggesting a positive relationship of the maar size with the depth of the diatreme–debris system.

Integrated field studies in deeply dissected maar–diatreme volcanoes and experimental work in the future may cast new light on the relationships of exposed vs. buried morphologies, parent processes and energy partitioning in this volcano type in order to capture the relevant conditions controlling the shift from effusive or mildly explosive magmatic activities to more hazardous hydromagmatic ones in monogenetic volcanism.

Acknowledgements We thank Greg Valentine, Karoly Németh, the Editor Michael Manga and the Executive Editor James White for constructive journal reviews of the manuscript.

References

Auer A, Martin U, Németh K (2007) The Fekete-hegy (Balaton Highland Hungary) "soft-substrate" and "hard-substrate" maar volcanoes in an aligned volcanic complex—implications for vent geometry, subsurface stratigraphy and the palaeoenvironmental setting. J Volcanol Geotherm Res 159:225–245

Austin-Erickson A, Büttner R, Dellino P, Ort MH, Zimanowski B (2008) Phreatomagmatic explosions of rhyolitic magma: experimental and field evidence. J Geophys Res 113:B11201. doi:10.1029/2008JB005731

Barberi F, Navarro JM, Rosi M, Santacroce R, Sbrana A (1988) Explosive interaction of magma with ground water: insights from xenoliths and geothermal drillings. Rend Soc Ital Mineral Petrol 43:901–926

Boni C, Bono P, Capelli G (1986) Schema idrogeologico dell'Italia Centrale. Mem Soc Geol It 35:991–1012

Büttner R, Dellino P, La Volpe L, Lorenz V, Zimanowski B (2002) Thermohydraulic explosions in phreatomagmatic eruptions as evidenced by the comparison between pyroclasts and products from molten fuel coolant interaction experiments. J Geophys Res 107:2277–2290

Campobasso C, Cioni R, Salvati L, Sbrana A (1994) Geology and paleogeographic evolution of a peripheral sector of the Vico and Sabatini volcanic complex, between Civita Castellana and Mazzano Romano (Latium, Italy). Mem Descr Carta Geol It 49:277–290

Campos Venuti M, Rossi RL (1996) Depositional facies in the Firiplaka rhyolitic tuff ring, Milos Island (Cyclades, Greece). Acta Vulcanol 8(2):47–63

Carrasco-Núñez G, Ort MH, Romero C (2007) Evolution and hydrological conditions of a maar volcano (Atexcac crater, eastern Mexico). J Volcanol Geotherm Res 159:179–197

Cas RAF, Wright JV (1987) Volcanic successions modern and ancient. Allen and Unwin, London, p 528

Cioni R, Laurenzi MA, Sbrana A, Villa IM (1993) $^{40}Ar/^{39}Ar$ chronostratigraphy of the initial activity in the Sabatini volcanic complex (Italy). Boll Soc Geol It 112:251–263

Civitelli G, Corda L (1993) The allochthonous succession. In: Di Filippo M (ed) Sabatini volcanic complex. Quad Ric Sci, vol 114. Progetto Finalizzato Geodinamica CNR, Rome, pp 19–28

Colucci S, Palladino DM, Simei S, Sottili G (2010) Magmatic vs. hydromagmatic fragmentation and its bearing on the origin of widely dispersed ash deposits. Abs Cities on Volcanoes 6, 31 May–4 June 2010, Puerto de la Cruz, Tenerife, Spain, p 23

Conticelli S, Francalanci L, Manetti P, Cioni R, Sbrana A (1997) Petrology and geochemistry of the ultrapotassic rocks from the Sabatini Volcanic District, central Italy: the role of evolutionary processes on the genesis of variably enriched alkaline magmas. J Volcanol Geotherm Res 75:107–136

Cundari A (1979) Petrogenesis of leucite-bearing lavas in the Roman volcanic region, Italy. The Sabatini Lavas. Contrib Mineral Petrol 70:9–21

De Astis G, Pappalardo L, Piochi M (2004) Procida volcanic history: new insights into the evolution of the Phlegrean Volcanic District (Campanian region, Italy). Bull Volcanol 66:622–641

Dellino P, La Volpe L (1995) Fragmentation versus transportation mechanisms in the pyroclastic sequence of Monte Pilato-Rocche Rosse (Lipari, Italy). J Volcanol Geotherm Res 64:211–231

Dellino P, La Volpe L (1996) Cluster analysis on ash particles morphology features to discriminate fragmentation dynamics in explosive eruptions. Acta Vulcanol 8–1:31–39

de Rita D, Sposato A (1986) Correlazione tra eventi esplosivi e assetto strutturale del substrato sedimentario nel complesso vulcanico Sabatino. Mem Soc Geol It 35:727–733

de Rita D, Zanetti G (1986) I centri esplosivi di Baccano e Stracciappe (Sabatini orientali, Roma): analogie e differenze della modellistica esplosiva in funzione del grado di interazione acqua/magma. Mem Soc Geol It 35:689–697

de Rita D, Funiciello R, Corda L, Sposato A, Rossi U (1993) Volcanic units. In: Di Filippo M (ed) Sabatini volcanic complex. Quad Ric Sci, vol 114. Progetto Finalizzato Geodinamica CNR, Rome, pp 33–79

Devine JD, Gardner JE, Brack HP, Layne GD, Rutherford MJ (1995) Comparison of microanalytical methods for estimating H_2O contents of silicic volcanic glasses. Am Mineral 80:319–328

Di Filippo M, Toro B (1993) Gravimetric study of Sabatini area. In: Di Filippo M (ed) Sabatini volcanic complex. Quad Ric Sci, vol 114. Progetto Finalizzato Geodinamica CNR, Rome, pp 95–99

Di Vito MA, Arienzo I, Braia G, Civetta L, D'Antonio M, Di Renzo V, Orsi G (2010) The Averno 2 fissure eruption: a recent small-size explosive event at the Campi Flegrei Caldera (Italy). Bull Volcanol 73:295–320. doi:10.1007/s00445-010-0417-0

Dolfi D, Palladino DM, Trigila R, Zanon V (2011) Aspetti chimico-petrografici e geocronologici delle vulcaniti della Media Valle Latina. In: Centamore E (ed) Note Illustrative della Carta Geologica d'Italia, Foglio 402 "Ceccano" (in press)

Ernst GGJ, Carey SN, Bursik MI, Sparks RSJ (1996) Sedimentation from turbulent jets and plumes. J Geophys Res 101:5575–5589

Fagents SA, Wilson L (1993) Explosive volcanic eruptions, VII. The ranges of pyroclasts ejected in transient volcanic explosions. Geophys Int 113:359–370

Fagents SA, Wilson L (1996) Numerical modeling of ejecta dispersal from transient volcanic explosions on Mars. Icarus 123:284–295

Foley SF, Venturelli G, Green DH, Toscani L (1987) The ultrapotassic rocks: characteristics, classifications and constraints for petrogenetic models. Earth Sci Rev 24:81–134

Franzini M, Leoni M, Saitta M (1972) A simple method to evaluate the matrix effects in X-ray fluorescence analysis. Spectrometry 1:151–154

Funiciello R, Mariotti G, Parotto M, Preite-Martinez M, Tecce F, Toneatti R, Turi B (1979) Geology, mineralogy and stable isotope geochemistry of the Cesano geothermal field (Sabatini Mts. Volcanic system, Northern Latium, Italy). Geothermics 8:55–73

Gaeta M, Di Rocco T, Freda C (2009) Carbonate assimilation in open magmatic systems: the role of melt-bearing skarns and cumulate-forming processes. J Petrol 50:361–385

Giaccio B, Sposato A, Gaeta M, Marra F, Palladino DM, Taddeucci J, Barbieri M, Messina P, Rolfo MF (2007) Mid-distal occurrences of the Albano Maar pyroclastic deposits and their relevance for reassessing

the eruptive scenarios of the most recent activity at the Colli Albani Volcanic District, Central Italy. Quat Int 171–172:160–178
Giardini M (2007) Late Quaternary vegetation history at Stracciacappa (Rome, central Italy). Vegetation History and Archaeobotany 16 (4):301–316
Goto A, Taniguchi H, Yoshida M, Ohba T, Oshima H (2001) Effect of explosions energy and depth to the formation of blast wave and crater: field explosion experiment for the understanding of volcanic explosion. Geophys Res Lett 28:4287–4290
Head JW, Sparks RSJ, Bryan WB, Walker GPL, Greely R, Whitford-Stark JL, Guest JE, Wood CA, Shultz PH, Carr MH (1981) Distribution and morphology of basalt deposits on planets. In: Project BVS (ed) Basaltic volcanism on the terrestrial planets. Pergamon, New York, pp 701–800
Heiken G, Wohletz K (1985) Volcanic ash. University of California Press, Berkeley, 246 pp
Houghton BF, Wilson CJN (1989) A vesicularity index for pyroclastic deposits. Bull Volcanol 51:451–462
Houghton BF, Wilson CJN, Rosenberg MD, Smith IEM, Parker RJ (1996) Mixed deposits of complex magmatic and phreatomagmatic volcanism: an example from Crater Hill, Auckland, New Zealand. Bull Volcanol 58:59–66
Houghton BF, Wilson CJN, Smith RT, Gilbert JS (2000) Phreatoplinian eruptions. In: Sigurdsson H (ed) Encyclopedia of volcanoes. Academic, San Diego, pp 513–525
Kano K, Ohguchi T (2009) Intra-crater deposits of the Toga tuff ring, Oga Peninsula, NE Japan. Sed Geol 220:204–217
Kano K, Ohguchi T, Hayashi S, Uto K, Danhara T (2002) Toga volcano: an alkali-rhyolite tuff-ring in the western end of Oga Peninsula, NE Japan. Bull Volcanol Soc Japan 47(5):373–396
Karner DB, Marra F, Renne P (2001) The history of the Monti Sabatini and Alban Hills volcanoes: groundwork for assessing volcanic–tectonic hazards for Rome. J Volcanol Geotherm Res 107:185–219
Laurenzi MA, Villa IM (1987) $^{40}Ar/^{39}Ar$ chronostratigraphy of the Vico ignimbrites. Per Mineral 56:285–293
Lorenz V (1971) An investigation of volcanic depressions. Part IV. Origin of Hole-in-the-Ground, a maar in Central Oregon (Geological, geophysical and energy investigations). Prog Rep NGR-38-003-012, NASA, Houston, TX, 113 pp
Lorenz V (1973) On the formation of maars. Bull Volcanol 37:183–204
Lorenz V (1986) On the growth of maars and diatremes and its relevance to the formation of tuff-rings. Bull Volcanol 48:265–274
Lorenz V (2003) Maar–diatreme volcanoes, their formation, and their setting in hard-rock or soft-rock environments. Geolines—J Geol Inst AS Czech Republic 15:72–83
Lorenz V (2007) Syn- and posteruptive hazards of maar–diatreme volcanoes. J Volcanol Geotherm Res 159:285–312
Mariotti G (1993) Basal carbonate succession. In: Di Filippo M (ed) Sabatini volcanic complex. Quad Ric Sci, vol 114. Progetto Finalizzato Geodinamica CNR, Rome, pp 11–18
Masotta M, Gaeta M, Gozzi F, Marra F, Palladino DM, Sottili G (2010) H_2O- and temperature-zoning in magma chambers: the example of the Tufo Giallo della Via Tiberina eruptions (Sabatini Volcanic District, central Italy). Lithos 118:119–130
Mastin LG (1991) The roles of magma and groundwater in the phreatic eruptions at Inyo Craters, Long Valley Caldera, California. Bull Volcanol 53:579–596
Mastrolorenzo G, Brachi L, Canzanella A (2001) Vesicularity of various types of pyroclastic deposits of Campi Flegrei volcanic field: evidence of analogies in magma rise and vesiculation mechanisms. J Volcanol Geotherm Res 109:41–53
Moore G, Vennemann T, Carmichael ISE (1998) An empirical model for the solubility of H_2O in magmas to 3 kilobars. Am Mineral 83:36–42
Nappi G, Mattioli M (2003) Evolution of the Sabatinian Volcanic District (central Italy) as inferred by stratigraphic successions of its northern sector and geochronological data. Per Mineral 72:79–102
Németh K (2010) Monogenetic volcanic fields: origin, sedimentary record, and relationship with polygenetic volcanism. Geol Soc Am Spec Pap 470:43–66
Németh K, Cronin S, Haller M, Brenna M, Csillag G (2010) Modern analogues for Miocene to Pleistocene alkali basaltic phreatomagmatic fields in the Pannonian Basin: "soft-substrate" to "combined" aquifer controlled phreatomagmatism in intraplate volcanic fields. Centr Eur J Geosci 2(3):339–361
Ollier CD (1967) Maars: their characteristics, varieties and definition. Bull Volcanol 31:45–75
Palladino DM, Taddeucci J (1998) The basal ash deposit of the Sovana Eruption (Vulsini Volcanoes, central Italy): the product of a dilute pyroclastic density current. J Volcanol Geotherm Res 87:233–254
Palladino DM, Gaeta M, Marra F (2001) A large K-foiditic hydromagmatic eruption from the early activity of the Alban Hills VolcanicDistrict (Italy). Bull Volcanol 63:345–359
Palladino DM, Simei S, Kyriakopoulos K (2008) On magma fragmentation by conduit shear stress: evidence from the Kos Plateau Tuff, Aegean Volcanic Arc. J Volcanol Geotherm Res 178:807–817
Palladino DM, Simei S, Sottili G, Trigila R (2010) Integrated approach for the reconstruction of stratigraphy and geology of Quaternary volcanic terrains: an application to the Vulsini Volcanoes (central Italy). In Groppelli G, Viereck L (eds) Stratigraphy and geology in volcanic areas. Geol Soc Am Spec Pap 464, pp 66–84
Peccerillo A, Federico M, Barbieri M, Brilli M, Wu TW (2010) Interaction between ultrapotassic magmas and carbonate rocks: evidence from geochemical and isotopic (Sr, Nd, O) compositions of granular lithic clasts from the Alban Hills Volcano, Central Italy. Geochim Cosmochim Acta 74:2999–3022
Ross P-S, White JDL, Zimanowski B, Büttner R (2008) Multiphase flow above explosion sites in debris-filled volcanic vents: insights from analogue experiments. J Volcanol Geotherm Res 178:104–112
Ross P-S, Delpit S, Haller MJ, Németh K, Corbella H (2011) Influence of the substrate on maar–diatreme volcanoes—an example of a mixed setting from the Pali Aike volcanic field, Argentina. J Volcanol Geotherm Res 201:253–271. doi:10.1016/j.jvolgeores.2010.07.018
Sahagian DL, Proussevitch AA (1998) 3D particle size distributions from 2D observations: stereology for natural applications. J Volcanol Geotherm Res 84:173–196
Sato H, Taniguchi H (1997) Relationship between crater size and ejecta volume of recent magmatic and phreato-magmatic eruptions: implications for energy partitioning. Geophys Res Lett 24:205–208
Scherillo A (1941) Studi su alcuni tufi gialli della regione sabazia orientale. Per Mineral 12:381–417
Self S, Kienle J, Huot J-P (1980) Ukinrek Maars, Alaska. II. Deposits and formation of the 1977 craters. J Volcanol Geotherm Res 7:39–65
Sheridan MF, Wohletz KH (1983) Hydrovolcanism: basic considerations and review. J Volcanol Geotherm Res 17:1–29
Shimozuru D (1968) Discussion on the energy partition of volcanic eruption. Bull Volcanol 32:383–394
Sohn YK, Cough SK (1989) Depositional processes of the Suwolbong tuff ring, Cheju Island (Korea). Sedimentology 36:837–855
Sottili G, Palladino DM, Zanon V (2004) Plinian activity during the early eruptive history of the Sabatini Volcanic District, Central Italy. J Volcanol Geotherm Res 135:361–379
Sottili G, Taddeucci J, Palladino DM, Gaeta M, Scarlato P, Ventura G (2009) Sub-surface dynamics and eruptive styles of maars in the Colli Albani Volcanic District, Central Italy. J Volcanol Geotherm Res 180:189–202

Sottili G, Palladino DM, Marra F, Jicha B, Karner DB, Renne P (2010a) Geochronology of the most recent activity in the Sabatini Volcanic District, Roman Province, central Italy. J Volcanol Geotherm Res 196:20–30

Sottili G, Taddeucci J, Palladino DM (2010b) Constraints on magma–wall rock thermal interaction during explosive eruptions from textural analysis of cored bombs. J Volcanol Geotherm Res 192:27–34

Sparks RSJ, Walker GPL (1977) The significance of vitric-enriched air-fall ashes associated with crystal-enriched ignimbrites. J Volcanol Geotherm Res 2:329–341

Taddeucci J, Sottili G, Palladino DM, Ventura G, Scarlato P (2010) A note on maar eruption energetics: current models and their application. Bull Volcanol 72:75–83

Trigila R, Battaglia M, Manga M (2007) An experimental facility for investigating hydromagmatic eruptions at high-pressure and high-temperature with application to the importance of magma porosity for magma–water interaction. Bull Volcanol 69:365–372

Valentine GA, Shufelt NL, Hintz ARL (2011) Models of maar volcanoes, Lunar Crater (Nevada, USA). Bull Volcanol. doi:10.1007/s00445-011-0451-6

Walker GPL, Croasdale R (1972) Characteristics of some basaltic pyroclastics. Bull Volcanol 35:303–317

White JDL, Houghton B (2000) Surtseyan and related phreatomagmatic eruptions. In: Sigurdsson H (ed) Encyclopedia of volcanoes. Academic, San Diego, pp 495–513

White JDL, Ross P-S (2011) Maar–diatreme volcanoes: a review. J Volcanol Geotherm Res 201:1–29. doi:10.1016/j.jvolgeores.2011.01.010

Wohletz KH (1986) Explosive magma–water interaction: thermodynamics, explosive mechanisms, and field studies. Bull Volcanol 48:248–264

Wohletz KH (2002) Water/magma interaction: some theory and experiments on peperite formation. J Volcanol Geotherm Res 114:19–35

Wohletz KH (2003) Water/magma interaction: physical considerations for the deep submarine environment. In: White JDL, Smellie JL, Clague DA (eds) Explosive subaqueous volcanism. American Geophysical Union, Washington, pp 25–50

Wohletz KH, McQueen RG (1984) Volcanic and stratospheric dust-like particles produced by experimental water–melt interactions. Geology 12:591–594

Wohletz KH, Sheridan MF (1983) Hydrovolcanic explosions II: evolution of basaltic tuff rings and tuff cones. Am J Sci 283:385–413

Yokoo A, Taniguchi H, Goto A, Oshima H (2002) Energy and depth of Usu 2000 phreatic explosions. Geophys Res Lett 29:2195. doi:10.1029/2002GL015728

Yokoyama I, de la Cruz-Reyna S, Espindola JM (1992) Energy partition in the 1982 eruption of El Chichon volcano, Chiapas, Mexico. J Volcanol Geotherm Res 51:1–21

Zimanowski B, Büttner R (2003) Phreatomagmatic explosions in subaqueous volcanism. In: White JDL, Smellie JL, Clague DA (eds) Explosive subaqueous volcanism. American Geophysical Union, Washington, pp 51–60

Zimmer BW, Riggs NR, Carrasco-Núñez G (2010) Evolution of tuff ring–dome complex: the case study of Cerro Pinto, eastern Trans-Mexican Volcanic Belt. Bull Volcanol 72:1223–1240. doi:10.1007/s00445-010-0391-6